MPAE-W-46-79-11

THE MODIFICATION OF THE ANTENNA ARRAY AND THE DETERMINATION OF THE HEATING FREQUENCY FOR THE REALIZATION OF HEATING ROCKET EXPERIMENTS

G. Rose

MAX-PLANCK-INSTITUT FÜR AERONOMIE

THE MODIFICATION OF THE ANTENNA ARRAY AND THE DETERMINATION OF THE HEATING FREQUENCY FOR THE REALIZATION OF HEATING ROCKET EXPERIMENTS

Gerhard Rose

Max-Planck-Institut für Aeronomie, Postfach
3411 Katlenburg-Lindau 3
F.R.G.

The Modification of the Antenna Array and the Determination of the Heating Frequency for the Realization of Heating Rocket Experiments

The "HERO" (heating rocket) experiments are designed to measure in F-region heights some of the modifications of the natural ionospheric plasma which are produced in a height range of about 10 km thickness from closely below up to the reflection level of a very powerful heating radio wave [1, 2].

One of the problems arising immediately before the execution of such a rocket experiment is to determine the necessary heating frequency - e.g. on the basis of EISCAT electron density data measured at the same time - in order to make sure that the rocket will really reach the heated region or, to be on the safe side just will pass it twice on its way up and down as well.

Another point to be considered is the magnitude of the parameter $X = f_o^2 / f^2$ at the height of reflection. X_r must be greater than about 0.9 in order to avoid excessively high Landau damping [3]. Landau damping decreases very rapidly for $X > 0.9$ making the observation of plasma waves possible near the reflection level provided the wave is not too far from vertical incidence.

Further, for maximum heating the diagram of the relevant antenna array has to be adjusted at the same time so to obtain maximum power gain for that part of the reflection level which is closest to the apogee of the rocket.

The rockets shall be launched from Haugnes which is located in the north of the Norwegian island of Andoya. They can be launched almost parallel to the Norwegian coast line, which means

an azimuthal direction of about 35° east of north. In that case the maximum angle of elevation is limited to 83° because of security considerations. Under these conditions the instrumented rocket is expected to reach its apogee at a height of appr. 280 km in a distance of about 92 km north east of Haug-nes. From the heating site at Ramfjordmoen near Tromsø the azimuthal direction to the apogee is about 57.8° west of north at a distance of about 76 km, see Fig. 1.

In the first part of this paper the necessary modification of one of the available antenna arrays is outlined. In the second part the determination of the heating frequency is considered. Calculations including the earth magnetic field and the earth curvature are compared to more simple calculations which were obtained when the earth magnetic field and the earth curvature were neglected. By introducing "equivalent linear layers" a crude estimate of the heating frequency can easily be obtained very straightforward.

The relative frequency variation necessary for 1 km of height variation of the reflection level is considered there as well. This was done for different linear, parabolic and exponential layers so to obtain a measure for the stability of the reflection level.

The calculations including the earth magn. field were performed by using a rather sophisticated but versatile computer program of R.M. Jones and Judith J. Stephenson [4]. Their program was only slightly modified by attaching a "homing in" procedure in order to calculate frequency, initial zenith distance and initial azimuth angle of the relevant o. mode ray path which has to be

reflected - under the given ionospheric conditions - at the wanted point in the ionosphere in order to be sure that the reflection level and with it the heated region is just in the right position for the rocket. The above program was intensively tested before it was used. The additional programming was done by D. Stratmann. Another special ray tracing program of Bruce L. Cragin [5] is available to compare measurements with theory after the rocket launches have been performed.

However, any such calculations are only more or less realistic in the sence that they are based on the limited accuracy and resolution of the initial experimental electron density profile data. Moreover, deviations caused by horizontal gradients of the electron density are difficult to consider and would hardly improve the results from the experimental point of view; fortunately the HERO experiments are planned to be carried out during undisturbed conditions when horizontal gradients are not expected to play a dominant role.

The Modification of the Relevant Antenna Array

The antenna equipment of the heating facility at Ramfjordmoen near Tromsø [1] consists of three quadratic antenna arrays, each of which contains 6x6 crossed full wave dipoles. The gain of each array is about 24 dBi and the frequency ranges of the different arrays are: 2.75 - 4.00 MHz, 3.85 - 5.65 MHz and 5.50 - 8.00 MHz.

In order to be able to radiate waves of a given polarization each row of an array will be fed by two transmitters with the phase differences between the different dipoles composing the crosses adjustable. And by adjusting the phase differences between the transmitters of each row the beam can be steered

within the meridional plane.

For optimum power gain during the HERO experiments, however, the heating beam of the relevant antenna array has to be steered out of the meridional plane in order to beam into the direction of the rocket apogee as it appears through the ionosphere.

According to a preliminary study of the ionospheric conditions to be expected near Tromsø during the time of the experiments (which are planned to be carried out after sunset in the F-region near the equinoxes in 1981) it is assumed that the second array which ranges from 3.85 MHz to 5.65 MHz has to be modified.

Because one part of the phase difference necessary between the individual antenna elements for aiming into the wanted direction is immediately available from the adjustable phase differences between the rows of the array, it is only the remaining part which has to be adjusted by means of suitable delay lines. This means, as will be shown later, that delay lines are needed only for $(n-1)\cdot n$ antennas located in $(n-1)$ of the n columns of the array. The lengths of these lines being constant within a column.

For technical reasons and in order to reduce the expense it is intended to use in parallel each two of the six crossed dipoles of a row. The array would thus consist of six rows and three columns with the individual elements being two crossed full wave dipoles in parallel. Each such new element has two separate delay lines of the same length and two energy lines to the associated transmitters enabling to adjust for the wanted wave polarization as before.

The configuration of the array elements of the medium array can be seen from Fig. 2. The distances d_x between the rows is 46 m and between the centres of the columns is d_y = 92m.

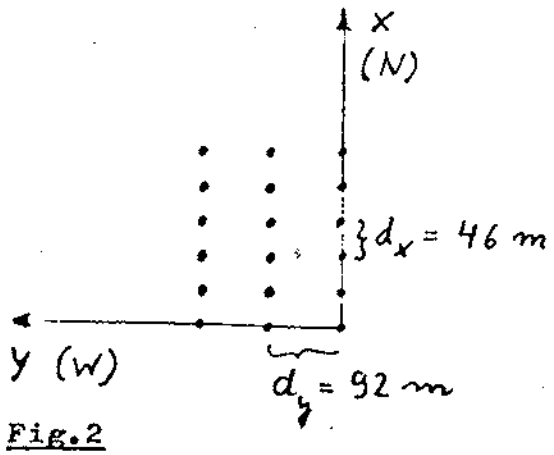

Fig.2

The length of the delay lines necessary for the individual elements to point the array beam into the wanted direction - characterized by the zenith distance θ_0 and the azimuth angle φ_0 - can be calculated in the following way (assuming the array elements to radiate isotropically, which is roughly true for small zenith distances, say $< 10^\circ \ldots 15^\circ$):

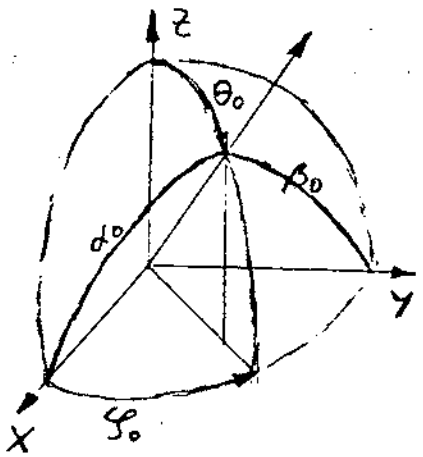

Fig.3

With θ_0 and φ_0 all the direction cosines, $\cos\alpha_0$, $\cos\beta_0$ and $\cos\theta_0$ are given, see Fig.3, the missing two are:

$$\cos\alpha_0 = \cos\varphi_0 \cdot \sin\theta_0$$
$$\cos\beta_0 = \sin\varphi_0 \cdot \sin\theta_0 \qquad (1)$$

The equation of the plane normal to the beam direction can be written:

$$x\cos\alpha_0 + y\cos\beta_0 + z\cos\theta_0 = 0, \qquad (2)$$

where the coordinate system is that given by Fig.3 (or by Fig.2 when the z-axis is assumed to point vertically upwards).

If now the coordinates, e.g. $x_0 = md_x$, $y_0 = nd_y$, $z_0 = 0$, of an antenna element as given by Fig.2 are introduced into (2) the distance of that element from the plane vertical to the beam direction is obtained. It is equivalent to the electrical length of the delay line needed for the array element under consideration if the geometry as given by Fig.2 and Fig. 3 applies. The cable lengths are given by Table 1:

$5d_x\cos\alpha_0 + 2d_y\cos\beta_0$	$5d_x\cos\alpha_0 + d_y\cos\beta_0$	$5d_x\cos\alpha_0$
$4d_x\cos\alpha_0 + 2d_y\cos\beta_0$	$4d_x\cos\alpha_0 + d_y\cos\beta_0$	$4d_x\cos\alpha_0$
$3d_x\cos\alpha_0 + 2d_y\cos\beta_0$	. .	.
$2d_x\cos\alpha_0 + 2d_y\cos\beta_0$	. .	.
$d_x\cos\alpha_0 + 2d_y\cos\beta_0$	$d_x\cos\alpha_0 + d_y\cos\beta_0$	$d_x\cos\alpha_0$
$2d_y\cos\beta_0$	$d_y\cos\beta_0$	0

Evidently, the first term in each row of Table 1 can be compensated by the existing array equipment as mentioned before when a suitable phase difference between the elements of neighbouring rows is introduced. This compensating phase difference is:

$$\Delta\varphi = \frac{2\pi}{\lambda} d_x \cos\alpha_o \ [\text{rad}], \text{ or}$$

$$\Delta\varphi = \frac{360^o}{c} d_x f \cos\alpha_o [\text{deg.}].$$

After that compensation the remaining lengths of the delay lines for the elements of the three columns of the array are: zero for the first column with y =0, $d_y \cos\beta_o$ for the column with $y = d_y$ and $2d_y \cos\beta_o$ for the column with $y = 2d_y$.

In order to calculate the diagram of the modified antenna array a method given by M.T. Ma [6] can largely be followed:

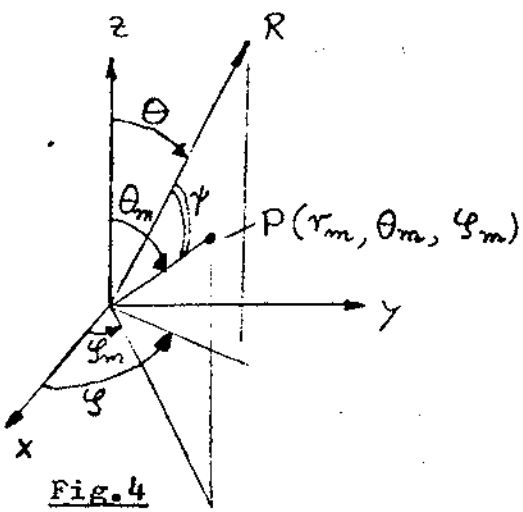

Fig. 4

In Fig. 4 the position P of an individual antenna is given in spherical coordinates: $P(r_m, \theta_m, \varphi_m)$. Further the direction to a point at very great distance (R) is indicated by the associated polar distance θ and the azimuth angle φ .

If now 'I' is the amplitude and α_m the phase excitation of the antenna at P, if further $f(\theta, \varphi)$ is its amplitude diagram, then the excitation in the point at distance R is:

$$E = f(\theta, \varphi) \cdot I \cdot e^{j(\omega t + \alpha_m - k(R - r_m \cos\gamma_m))}$$

$$= f(\theta, \varphi) \cdot I \cdot e^{j(kr_m \cos\gamma_m + \alpha_m)} \cdot e^{j(\omega t - kR)}, \qquad (3)$$

which means that the far field excitation produced by the antenna in P can be described by:

$$E = f(\theta, \varphi) \cdot I \cdot e^{j(kr_m \cos\gamma + \alpha_m)} \qquad (3a)$$

where $\cos\gamma$ is given by:

$$\cos\gamma = \cos\theta\cos\theta_m + \sin\theta\sin\theta_m\cos(\varphi - \varphi_m) \qquad (4)$$

If now the m individual antennas of a linear array were arranged e.g. along the x-axis at the points $x_1 = 0$, $x_2 = d_x$, $x_3 = 2d_x$, ... $x_m = (m-1)\cdot d_x$, then r_m is equal to 0, d_x, $2d_x$ ... $(m-1)d_x$ depending on the antenna considered and $\cos\gamma$ is:

$$\cos\gamma = \sin\theta\cos\varphi. \qquad (5)$$

For n antennas along the y-axis with the distance between neighbouring elements $d = d_y$ one correspondingly obtains that r_m can assume 0, d_y, $2d_y$ ... $(n-1)\cdot d_y$ and $\cos\gamma$ is:

$$\cos\gamma = \sin\theta\sin\varphi. \qquad (6)$$

Consequently the far field excited by m antennas of the same kind along the x-axis is:

$$E_{x,y=0} = f(\theta,\varphi)\cdot\sum_{\nu=0}^{m-1} I_\nu\, e^{j(\nu k d_x \sin\theta\cos\varphi + \alpha_\nu)} \qquad (7)$$

and the far field excited by n antennas along the y-axis is:

$$E_{x=0,y} = f(\theta,\varphi)\cdot\sum_{\mu=0}^{n-1} I_\mu\, e^{j(\mu k d_y \sin\theta\sin\varphi + \alpha_\mu)}. \qquad (8)$$

In the following α_ν (or α_μ respectively) are not assumed arbitrary but:

$$\alpha_\nu = -\nu k d_x \sin\theta_0\cdot\cos\varphi_0 \qquad (9)$$

and

$$\alpha_\mu = -\mu k d_y \sin\theta_0\cdot\sin\varphi_0. \qquad (10)$$

With these phase angles the far field of m isotropic antennas along the x-axis with constant amplitude but with the phase excitations according to (9) is:

$$E_{iso(x,y=0)} = f\cdot I\cdot\sum_{\nu=0}^{m-1} e^{j\nu k d_x(\sin\theta\cdot\cos\varphi - \sin\theta_0\cdot\cos\varphi_0)} \qquad (7a)$$

and the far field of n isotropic antennas along the y-axis with the phase excitations according to (10) is:

$$E_{iso(x=0,y)} = fI\sum_{\mu=0}^{n-1} e^{j\mu kd_y(\sin\theta\cdot\sin\varphi - \sin\theta_0\cdot\sin\varphi_0)} \qquad (8a)$$

This means for both the linear arrays that each of it beams into the direction which is characterized by the polar distance θ_0 and the azimuth angle φ_0.

Generalizing one could consider the diagram of a linear array with its m equal elements e.g. along the x-axis, as if produced by a single point source with the same diagram as the array, which is located at its centre, provided the field is examined at a distance which is very much greater than $(m-1)d_x$; (otherwise the array diagram would depend on the distance as well).

Consequently one can understand the far field of a rectangular array as if produced by a linear array e.g. parallel to the y-axis with its individual elements being linear arrays parallel to the x-axis.

If the amplitude excitation I is the same in all the same m·n individual antennas of the array then the far field of such an m,n rectangular array is given by:

$$E(\theta,\varphi) = f(\theta,\varphi)\cdot I\cdot\sum_{\nu=0}^{m-1} e^{j\nu kd_x(\sin\theta\cdot\cos\varphi - \sin\theta_0\cos\varphi_0)}\cdot \sum_{\mu=0}^{n-1} e^{j\mu kd_y(\sin\theta\cdot\sin\varphi - \sin\theta_0\cdot\sin\varphi_0)} \qquad (11)$$

The array factor, that is the product of the two sums, has again a maximum for the direction θ_0, φ_0.

Introducing the magnitudes $\sqrt{\Sigma\cdot\Sigma^*}$ of the two above complex sums the (relative) polar diagram of the array is found to be:

$$D(\theta,\varphi) = f(\theta,\varphi)\cdot\frac{\sin\frac{m}{2}kd_x(\sin\theta\cdot\cos\varphi - \sin\theta_0\cdot\cos\varphi_0)}{\sin\frac{k}{2}d_x(\sin\theta\cdot\cos\varphi - \sin\theta_0\cdot\cos\varphi_0)}\cdot$$

$$\cdot\frac{\sin\frac{n}{2}kd_y(\sin\theta\cdot\sin\varphi - \sin\theta_0\cdot\sin\varphi_0)}{\sin\frac{k}{2}d_y(\sin\theta\cdot\sin\varphi - \sin\theta_0\cdot\sin\varphi_0)}, \qquad (12)$$

where k can be replaced by $k = (2\pi/c)\cdot f$. $D(\theta, \varphi)$ is composed of three factors which may be abbreviated to obtain:

$$D(\theta, \varphi) = f(\theta, \varphi)\, T_x(\theta, \varphi)\, T_y(\theta, \varphi) \qquad (12a)$$

As an example the relative polar diagrams for a 6,3-array consisting of 18 isotropic antennas in free space as sketched in Fig.5 are shown there for three different frequencies.

Next, in order to approximate the experimental conditions the polar diagram of a horizontal dipole parallel to the x-axis above perfectly conducting ground is considered, it is [7]:

$$f(\theta, \varphi) = \frac{\cos\left(\frac{2\cdot\pi\cdot l}{\lambda}\cdot\cos\varphi\sin\theta\right) - \cos\left(\frac{2\cdot\pi\cdot l}{\lambda}\right)}{\sqrt{1 - \cos^2\varphi\cdot\sin^2\theta}}\cdot 2\cdot\sin\left(\frac{2\cdot\pi\cdot h}{\lambda}\cdot\cos\theta\right). \qquad (13)$$

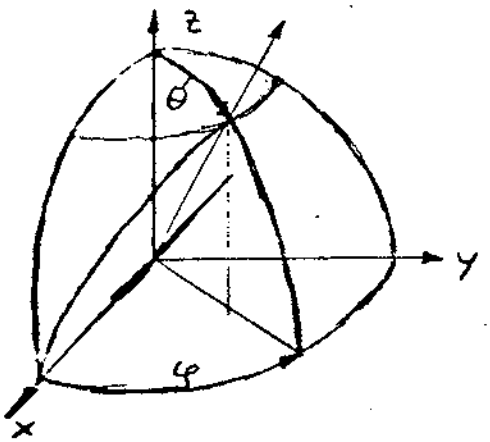

If two such dipoles are driven in parallel which are located on the y-axis, then their array factor $T_{(y)}$ (compare e.g. equ.(12)) can be determined. The far field diagram of such a double dipole with no phase difference between the two antennas is:

$$f_{2D}(\theta, \varphi) = f_D(\theta, \varphi)\cdot\frac{\sin(kd\cdot\sin\theta\sin\varphi)}{\sin\left(\frac{k}{2}d\cdot\sin\theta\sin\varphi\right)} = f_D\cdot T. \qquad (14)$$

The component $F_{\parallel}$ parallel to the plane of incidence can be shown to be:

$$F_{\parallel} = f_D(\theta, \varphi)\cdot\frac{\cos\theta}{\sqrt{\cos^2\theta + tg^2\varphi}}\cdot T = f_{\parallel}\cdot T \qquad (15)$$

and the component vertical to this plane is:

$$F_{\perp} = -f_D(\theta, \varphi)\cdot\frac{tg\,\varphi}{\sqrt{\cos^2\theta + tg^2\varphi}}\cdot T = f_{\perp}\cdot T \qquad (16)$$

Now we consider an m,n-array of crossed (full wave) double

dipoles as elements arranged in the way as mentioned earlier and as is roughly indicated in Fig.6. The angles between the axes of the different individual dipoles and the x-axis are $+45^{\circ}$ or -45° respectively.

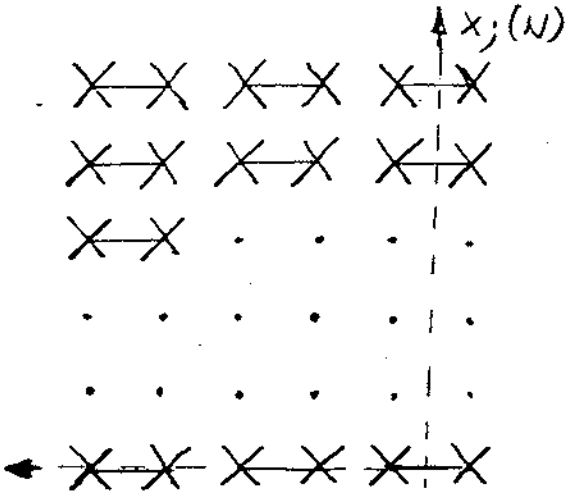

Fig.6

If an m,n-array is assumed to be composed of only the one kind of dipoles (with $+45^{\circ}$ orientation) the resulting relative diagram $D_{\parallel}$ for the component parallel to the plane of incidence is given by (see equ. (12), (12a) and (15)):

$$D_{\parallel}^{(+45)} = f_{\parallel}(\theta, \varphi - \tfrac{\pi}{4}) \cdot T(\theta, \varphi) \cdot T_x(\theta, \varphi) \cdot T_y(\theta, \varphi) \qquad (17)$$

and for the component vertical to the plane of incidence one obtains (see e.g. equ. (12), (12a) and (16)):

$$D_{\perp}^{(+45)} = f_{\perp}(\theta, \varphi - \tfrac{\pi}{4}) \cdot T(\theta, \varphi) \cdot T_x(\theta, \varphi) \cdot T_y(\theta, \varphi). \qquad (18)$$

If the array on the other hand were composed of only dipoles of -45° orientation, the relevant diagrams of it, $D_{\parallel}^{(-45)}$ and $D_{\perp}^{(-45)}$ were obtained in an obvious way when $f(\theta, \varphi - \frac{\pi}{4})$ in (17) and (18) were replaced by $f(\theta, \varphi + \frac{\pi}{4})$.

Again, the different factors in (17) and (18) are (with f_D, the diagram of the horizontal dipole above perfectly conducting ground, see equ. (13)):

$$f_{\parallel} = f_D(\theta, \varphi) \cdot \frac{\cos\theta}{\sqrt{\cos^2\theta + \mathrm{tg}^2\varphi}}, \qquad (19)$$

$$f_{\perp} = f_D(\theta, \varphi) \frac{tg\,\varphi}{\sqrt{\cos^2\theta + tg^2\varphi}}, \qquad (20)$$

$$T = \frac{\sin\,(kd \cdot \sin\theta \cdot \sin\varphi)}{\sin\,(\frac{k}{2}d \cdot \sin\theta \cdot \sin\varphi)} \qquad (21)$$

d is the distance between the dipoles in parallel and T_x and T_y are the second and the third factor of equ. (12) respectively with d_x and d_y being the relevant distances between the adjacent centres of the double dipoles.

If now the total array of m.n crossed double dipoles is excited in such a way that the phases between the dipoles composing a cross are in quadrature, then the diagram for each of the above-mentioned components (in the plane of incidence and vertically to it) is evidently obtained by summing the corresponding contributions from the two antennas of the crosses geometrically. Finally the total diagram of the array is obtained by again summing geometrically the two resulting components. One obtains:

$$D_{tot} = \sqrt{(D_{\parallel}(45))^2 + (D_{\parallel}(-45))^2 + (D_{\perp}(45))^2 + (D_{\perp}(-45))^2} \qquad (22)$$

In Figs. 7, 8 and 9 relative diagrams $f(\theta, \varphi \pm \varphi_0)$ (in dB above the relevant maximum) of a 6,3-array arranged in the way and with the dimensions as sketched in Fig.7 are drawn according to equ.(22) for different frequencies.

Because of the non-isotropic diagram of the individual double dipoles of the array, the relevant maximum is located at θ_m, φ_m instead at θ_0, φ_0 which is in our case only a slight shift of the order of a degree relative to θ_0, φ_0.

Figs.7 to 9 also contain the quotients between the wanted and the unwanted circular component of the radiated wave.

If "max" and "min" are the axes of the polarisation ellipse under consideration and if the vector composing this ellipse rotates in the sense of the wanted circular component one obtains:

$$\frac{\text{unwanted circ. comp.}}{\text{wanted circ. comp.}} = 20 \cdot \log \left(\frac{\text{max} - \text{min}}{\text{max} + \text{min}} \right) \qquad (23)$$

Considering the above outlined calculations one has to keep in mind that only approximations were obtained, on the one hand because of the assumption of a perfectly conducting ground, on the other because the current distributions along the antennas are expected to be different for single dipoles and the different dipoles located at different positions in the array. This last effect which is probably small but very difficult to take into account tends to flatten the array diagram a bit. In the same sense would a more realistic reflection coefficient tend to reduce the maximum gain of the system.

Relative to a 6,6-array being adjusted to point into a given direction, the 6,3-array composed of double elements as mentioned above certainly loses a bit of gain if pointed too far from out of the vertical because of the diagrams of its elements prefering the vertical direction. For our experiments, however, where angles of only about $\theta \approx 10^{\circ}$ are needed this loss is of no great importance but the reduction of expense is quite significant because of the fact that the cables going to the individual antennas are balanced coaxial, whereas each two of the dipoles are fed only by single coaxial cables, see Fig. 10.

If "max" and "min" are the axes of the polarisation ellipse under consideration and if the vector composing this ellipse rotates in the sense of the wanted circular component one obtains:

$$\frac{\text{unwanted circ. comp.}}{\text{wanted circ. comp.}} = 20 \cdot \log \left(\frac{\text{max} - \text{min}}{\text{max} + \text{min}} \right) \qquad (23)$$

Considering the above outlined calculations one has to keep in mind that only approximations were obtained, on the one hand because of the assumption of a perfectly conducting ground, on the other because the current distributions along the antennas are expected to be different for single dipoles and the different dipoles located at different positions in the array. This last effect which is probably small but very difficult to take into account tends to flatten the array diagram a bit. In the same sense would a more realistic reflection coefficient tend to reduce the maximum gain of the system.

Relative to a 6,6-array being adjusted to point into a given direction, the 6,3-array composed of double elements as mentioned above certainly loses a bit of gain if pointed too far from out of the vertical because of the diagrams of its elements prefering the vertical direction. For our experiments, however, where angles of only about $\theta \approx 10^{\circ}$ are needed this loss is of no great importance but the reduction of expense is quite significant because of the fact that the cables going to the individual antennas are balanced coaxial, whereas each two of the dipoles are fed only by single coaxial cables, see Fig. 10.

The Determination of the Heating Frequency

In order to be sure that the rocket with its given technical data will reach the heated region, one of the problems to be solved immediately before a HERO launch is the determination of the heating frequency which is the only parameter on which the level of reflection depends for a given ionosphere. This frequency is characterized by the fact, that a ray must exist which is reflected at the wanted point in the F-region which is located at (or better, slightly below) the apogee of the rocket.

Clearly, this problem can on principle be treated by a suitable computer program taking into account all the essential input data of which the electron density distribution has to be determined experimentally on line e.g. by EISCAT.

Of course such a program is rather involved. Moreover, it would be very difficult from the experimental and theoretical point of view to take e.g. inhomogeneities into account and to perform at the same time quasi on line homing in calculations. Therefore one has to be satisfied with approximate solutions anyway, keeping inhomogeneities and non-horizontal stratifications out of consideration.

To be on the safe side it would be very desirable to pre-heat the ionosphere using the computed frequency, which has to be corrected, if necessary according to EISCAT observations of the heated region to have it finally located in the wanted position relative to the prospected apogee of the rocket. This method, however, is limited by the fact that EISCAT is only fully steerable in case of UHF observations, which means in our case that plasma line observations are only possible for heating frequencies larger than about 6 MHz, because otherwise the scattering conditions for 933 MHz waves occur in a height where Landau damping

dominates [8]. Nevertheless should it be possible to search for the region of largest heat deposit vertically above the sub-apogee.

Because EISCAT observations of the really heated region appear to be very helpful and even necessary in any case, it would probably be sufficient to use a first order approximation of the heating frequency, keeping in mind that both the available computer programs of Cragin [5] and of Jones and Stephenson [4] which take the earth magnetic field into account are rather voluminous and probably difficult to handle with a sufficiently low computing time in northern Norway.

On the other hand is an accurate program later on absolutely necessary for the interpretation of the measurements. It is further necessary to compute for a realistic ionosphere as to be expected during the launch periods the average and the average variation of the frequency, of the initial zenith distance and of the azimuth angle of the rays leading to the heated region below the rocket apogee so to be able to modify the relevant antenna array accordingly.

Before going more into the details the most significant differences between the calculations taking the earth magnetic field into account and the estimations neglecting it shall be mentioned:

1.) The earth magnetic field introduces an azimuthal deviation of the ordinary ray to the north along its path to the vertex in the north-west of Ramfjordmoen. As a result the initial azimuth direction has to be more to the south compared to a ray remaining in the plane of incidence, if the given point in the ionosphere shall be reached.

2.) The initial zenith distance of a ray leading to the wanted point of reflection in the ionosphere is clearly smaller if the earth magnetic field is taken into account and if ordinary rays are considered, see Fig. 11.

3.) For a constant frequency the level of reflection of ordinary waves is higher which means that $X_r = f_{or}^2/f^2$ is greater compared to the corresponding no magnetic field approximation.

In the following the parameters frequency, initial zenith distance and initial azimuth angle are looked at. These parameters have been calculated for a given ionosphere and a ray which, as seen from the transmitting site, has its vertex at D = 76 km, h_r = 280 km and $\varphi = 57.8^\circ$ west of north. The above point corresponds approximately to the centre of the region which is to be heated during the rocket experiments, maybe it has to be a little lower later on depending on the performance of the instrumented rocket. Different parabolic layers and different critical frequencies (relative to the electron gyrofrequency) were considered.

In order to compare the differences in frequency, initial zenith distance and initial azimuth angle between the more accurate calculations and the approximations the above homing in procedures were always repeated for the same ionosphere when the earth magnetic field and the earth curvature were neglected.

The differences between the heights of reflection which were obtained when the earth magnetic field was included or not were calculated in the following way: When the earth magnetic field was included the frequency leading to the wanted point of reflection was calculated for the given ionosphere. Then, ignoring the earth magnetic field (and the earth curvature) the height of the reflection level at D = 76 km was determined again for

the same frequency.

Fig. 12 shows the results of the comparisons as far as height and frequency differencies are concerned. The lower the lower border h_o of the parabolic layer and the closer the point of reflection is located near the layer maximum the greater is the difference between the heights and frequencies obtained from the computations. There also exists a dependence of Δh and Δf on the quotient f_c/f_H as to be seen from Fig. 12. Both, Δh and $|\Delta f/f|$ (only Δf is represented in Fig. 12) decrease with increasing f_c/f_H.

As mentioned before one will really obtain a greater height in practice if the frequency is used which was computed without taking the earth magnetic field into account. To compensate for that, the frequency must consequently be lowered by Δf as shown in Fig. 12.

The differences $\Delta\varphi$ between the initial azimuth angles and between the initial zenith distances $(\Delta\theta)$ as obtained for different critical frequencies are shown in Fig. 13. Clearly, if the magnetic field is not taken into account the azimuth angle is that of the line of sight to the point in the ionosphere which is aimed at. Again, the lower the lower boundery of the parabolic layer and the closer the point of reflection is located to the layer maximum, the more does the initial azimuth angle deviate to the south relative to that of the line of sight if the wanted point of reflection shall be reached by the ray, see Fig. 13.

In the same sense are the initial zenith distances smaller for ray paths calculated with the earth magnetic field taken into account. The above-mentioned differences (see Fig. 13) are the smaller the higher the critical frequencies are relative to the electron gyrofrequency.

As mentioned before some useful information may be obtained from calculations which are rather easy to perform without taking the earth magnetic field into account. One of the problems is to know something about the stability of the reflection level at a fixed point with reference to small changes of the ionosphere. Therefore at first the frequencies $f_r = f/f_c$ *) were calculated for different linear, parabolic and exponential layers for which the level of reflection is located at a height h_r of 280 km above the expected sub-apogee of the rocket, that is at a distance of 76 km. Afterwards the quantity:

$$(1/f_r)\cdot(df_r/dh_r) \qquad (24)$$

was determined which is a measure of the relative frequency variation necessary to raise the reflection level by 1km of height at the point of consideration.

$(1/f_r)(df_r/dh_r)$ can be obtained by considering for a given (e.g. parabolic) layer the function:

$$F = D_s - D(h_o, Y_m, h_r, f_r), \qquad (25)$$

where D_s is the distance to the sub-apogee and D is the (horizontal) distance to the point of reflection, h_o and Y_m are the lower border and the half thickness (scale height) of the considered layer, $h_r = h_r(Y_m, \varphi_o, f_r)$ is the wanted height of reflection (where the ray is horizontal), f_r is the quotient between transmitter frequency and the critical frequency of the ionospheric layer and φ_o is the angle of incidence.

To obtain a numerical value for (24) the ray has at first to be homed in, that is the frequency f_r has to be determined for a given set of h_o, Y_m, h_r (=280km) for which F in equ.(25)

*) f_c is the crit. frequ. or the plama frequ. at a given height.

vanishes. Then, by numerical differentiation $(\partial D/\partial h_r)_{F=0}$ and $(\partial D/\partial f_r)_{F=0}$ have to be determined from which follows:

$$(1/f_r)(df_r/dh_r) = -(1/f_r)(\partial D/\partial h_r)/(\partial D/\partial f_r). \qquad (26)$$

The results of such calculations as obtained for linear and different parabolic layers are shown in Fig. 14. The closer the point of reflection (which was inspected at D = 76km, h_r = 280km) is located to the layer maximum (in case of a parabolic layer) and the farther the layer extends below that level (the smaller h_o is) the smaller is the relative frequency variation which causes 1km of height variation of the reflection level at the point of inspection.

In case e.g. of curve 4 of Fig. 14 the relative frequency (which is not indicated there) is always such that the reflection level at D = 76km is 20km below the layer maximum which is located at h_m = 300km. If the lower border of that parabolic layer is assumed to be at h_o = 220km, which corresponds to a layer half thickness of Y_m = 80km, the value of $(1/f_r)(df_r/dh_r)$ is found to be about $2.85 \cdot 10^{-3}\text{km}^{-1}$. As indicated in Fig. 14 the corresponding value of X at the point of reflection is $X_r \approx 0.962$ which is equivalent to a heating frequency of $f = f_o(280\text{km})/\sqrt{X_r}$.

The relation between the heating frequency leading to h_r = 280km at D = 76km and the critical frequency of the parabolic layer can be obtained by introducing:

$$f_e^2 = f_c^2(1 - (y/Y_m)^2)$$

and one has:

$$f_r = f/f_c = \sqrt{\frac{1 - (y_r/Y_m)^2}{X_r}}.$$

In the above example is y_r = 20km and Y_m = 80km, so $f_r \approx 0.987$. In case of a critical frequency of e.g. f_c = 4MHz a heating frequency of 3.949MHz results and the frequency variation per km of height variation is: $\pm\ 2.85 \cdot 10^{-3}\text{km}^{-1} \cdot 3.949\text{MHz} \approx \pm 11.3\text{kHz/km}$. (again: $h_r \approx$ 280km $\pm$ 1km at D = 76km for 3.949MHz $\pm$ 11.3kHz when f_c = 4MHz, h_o = 220km, Y_m = 80km).

If, on the other hand in case of curve 4 of Fig. 14, h_o is taken 100km, the corresponding values are found to be $(1/f_r)(df_r/dh_r) \approx 3.3 \cdot 10^{-4}\text{km}^{-1}$, $X_r \approx 0.988$ and $f_r \approx 1.001$. The heating frequency would be 4.004MHz for 4MHz critical frequency and the frequency variation per km of height variation is $\pm$ 3.3 10^{-4}km^{-1}. 4.004MHz $\approx \pm$ 1.32kHz/km at the above-mentioned point of reflection.

The consequences to be drawn from Fig. 14 are the following: Experimental difficulties are to be expected if $(1/f_r)(df_r/dh_r)$ is too small e.g. when significant changes of the reflection level are to be expected during the interval between the last determination of the heating frequency and the time when the rocket reaches its apogee. This may occur if the reflection level is located rather close to the maximum of the (parabolic) layer and when at the same time h_o is far below.

Of coarse, X_r is rather large in that case which would highly be appreciable. But on the other hand are rather small changes of the ratio f/f_c accompanied by rather big changes of the height of reflection which could move the heated region out of the range of the rocket if the layer is slightly variable during the experiment.

In Fig. 15 $(1/f_r)(df_r/dh_r)$ is shown as a function of α for different exponential layers $f_o^2 = f_o^2(h_o) \cdot e^{\alpha \cdot (h - h_o)}$, ($h_o$ is a

reference height). In case of Fig.15 f_r was taken $f_r = f/f_o(h_o)$. Compared to the different parabolic layers the level of reflection is found to be more stable with reference to small changes of f_r for exponential layers.

Because of the above stability considerations one would hardly start a rocket if the level of reflection is too close to an ionisation maximum, that is when small changes of the ionosphere are accompanied by rather large variations of the reflection level. Excluding these conditions and neglecting as before the earth magnetic field one can obtain, however, a very straight forward approximation of the heating frequency which is to be reflected as necessary at the wanted point in the F-region.

The method is to replace the given electron profile by an "equivalent linear layer" which is the linear profile that coincides with the given profile at the level of reflection having at the same time the same electron content up to that height level as well.

As will be shown in the appendix the angle of incidence of an electromagnetic wave which is reflected at the point D,h_r in any linear layer is given by:

$$\varphi_o = \operatorname{arctg} \frac{D}{2h_r - h_{oL}} \quad ; \quad h_r > h_o \qquad (27)$$

(h_{oL} is the lower border of the (equivalent) linear layer) and the relation between the plasma frequency at the height of reflection f_{or} and the heating frequency (with the quality to be reflected at the point D,h_r) is:

$$f_h = f_{or}/\cos\varphi_o . \qquad (28)$$

If the relevant electron profile has been determined experimentally up to the wanted height of reflection, f_{or} is known

and the missing h_{oL} can be calculated by numerical integration to obtain (as will be shown in the appendix):

$$h_{oL} = h_r - \frac{2}{f_{or}^2} \cdot \int_0^{h_r} f_o^2(h)\,dh \qquad (29)$$

With the aid of equ. (29) and (27) equ. (28) immediately yields the wanted heating frequency.

It is interesting to compare the heating frequencies which were obtained from the above (exactly integrated) approximations with the exact solutions for the different layers under consideration. As before, the earth magnetic field was neglected and the heating frequencies were determined to have the point of reflection located at D = 76 km, h_r = 280 km.

Fig.16 shows the quotients "CORR" between the exact solutions for the heating frequency and the approximations for different parabolic layers. Clearly, the higher the layer maximum is located above the level of reflection the more does the correction term CORR tend to unity. But even in case the reflection level is only 20km below the layer maximum (see the two lowest curves of Fig.16 most to the left, where h_o is 180km or 200km respectively) the difference between the exact solutions for f_h and the approximations is not greater than about 4‰ to 5‰ for the two presented curves.

Fig. 17 shows the corresponding results of calculations obtained for different exponential layers. The approximated heating frequencies tend to be a bit too low in this case.

The differences between the levels of reflection at D =76 km for the approximated and the exact heating frequencies are presented in Fig.18 for different parabolic layers. (For the

exact solution is h_r again always 280 km at D =76 km). As to be seen from Fig.18 the differences are the greater the nearer the reflection level is located to the layer maximum and the lower the lower boundery is below h_r. Clearly, a maximum of ionization cannot be represented by any linear layer.

The corresponding height of reflection differences at D= 76km as obtained for the approximate equivalent linear layer solutions and the exact solution (h_r =280 km at D =76 km) for exponential layers are shown in Fig.19. As to be seen, Δh_r is much smaller compared to the differences of the reflection heights as obtained for parabolic layers. Further, the heights of reflection belonging to the approximate heating frequencies are smaller than the wanted height of reflection.

In Figs. 20 and 21 three neighbouring rays and the levels of reflection are drawn for a parabolic (Fig.20) and an exponential layer (Fig.21). The dashed lines in these figures indicate the positions of the reflection levels as obtained for the relevant linear layer approximations.

From the above considerations it may be concluded that equivalent linear layer approximations are quite useful in some cases. Significant differences, however, are to be expected when the wanted point of reflection is located at a level close to an ionization maximum or near a point of inflection (or (and) when it is located very high above the lower border of the (non-linear) layer). If these restrictions do not apply even the results obtained from the more accurate calculations with the earth magnetic field included tend to be not too different from the simple estimations for the same layer without the field (see Figs. 12 and 13).

Therefore, whenever there is a possibility to check the height

of the heated region on line by use of a suitable groundbased experiment as EISCAT maybe, one of the more simple approximations of the heating frequency could be helpful.

Finally, a simple formula shall be mentioned to estimate the ratio X at the height of reflection. This formula is also derived in the appendix. If the earth magnetic field is neglected and a linear layer is considered a very simple relation exists between $X_r = [f_o^2/f^2](h_r)$ and the (horizontal) distance D to the vertex of the ray at h_r in the ionosphere. If

$$D \leq \frac{1}{3}(2h_r - h_o), \qquad h_o < h_r$$

(h_o is the lower border of the linear layer)
the frequency of the ray leading to the vertex D, h_r -which can be estimated with the aid of (27) and (28)- is such that

$$X_r = [f_o^2/f^2](h_r) \geq 0.9 \ ,$$

a condition for which Landau damping can be neglected [8].

Acknowledgements

The author is indebted to J.A. Fejer, H. Kopka, D. Stratmann and P. Stubbe for valuable discussions. The "HERO" rocket program is supported by the Bundesminister für Forschung und Technologie.

Appendix

In the following some of the equations which have been used in this paper shall be derived. The ray tracing program including the earth magnetic field, however, has been described in detail already in the relevant paper of Jones and Stephenson [4]. Therefore only the homing in procedure is sketched below. The other calculations do not include the earth magnetic field. In spite of that, some quite useful relations - as shown in the first part of this paper - are obtained.

Principle of the Homing in Procedure

Ray tracing programs are designed to determine among others the coordinates $X_r, Y_r, Z_r(f, \Theta, \varphi)$ of the point of reflection for a ray in the given (horizontally stratified) ionosphere of which the parameters: frequency f, initial zenith distance Θ and initial azimuth angle φ are known. Homing in means in our case to determine the parameters f, Θ, φ of a ray such that its point of reflection coincides with a given aiming point X_o, Y_o, Z_o. Therefore the parameters f, Θ, φ have to be determined such that the three functions

$$\begin{aligned} \Delta X &= X_r(f, \Theta, \varphi) - X_o \\ \Delta Y &= Y_r(f, \Theta, \varphi) - Y_o \\ \Delta Z &= Z_r(f, \Theta, \varphi) - Z_o \end{aligned} \qquad (30)$$

vanish simultaneously, which means in practice that they have to be smaller than three given small values.

For an initially estimated triple f, Θ, φ the above functions $\Delta X, \Delta Y, \Delta Z$ are calculated with the ray tracing program and, at the same time, numerical values of the nine derivatives $(\Delta X)_f$, $(\Delta Y)_f$ ... $(\Delta Z)_\varphi$ are determined ($(\Delta X)_f \ldots (\Delta Z)_\varphi$ are identical with $(X_r)_f$ ...

$(Z_r)_\varphi$ because $X_o, Y_o Z_o$ are constants). This can be done as indicated by the following example:

$$(X_r)_\theta \approx \frac{(X_r)(f, \theta\cdot(1 + 10^{-4}), \varphi) - (X_r)(f, \theta, \varphi)}{\theta \cdot 10^{-4}}$$

When all these quantities are known one has three linear equations to determine $\Delta f, \Delta\theta, \Delta\varphi$ by which the initial values have to be corrected to obtain the better approach $f + \Delta f$, $\theta + \Delta\theta$ and $\varphi + \Delta\varphi$. These three equations are:

$$\begin{aligned}
(X_r)_f \Delta f + (X_r)_\theta \Delta\theta + (X_r)_\varphi \Delta\varphi &= -\Delta X \\
(Y_r)_f \Delta f + (Y_r)_\theta \Delta\theta + (Y_r)_\varphi \Delta\varphi &= -\Delta Y \qquad (31) \\
(Z_r)_f \Delta f + (Z_r)_\theta \Delta\theta + (Z_r)_\varphi \Delta\varphi &= -\Delta Z
\end{aligned}$$

The above calculations for improving f, θ, φ can be repeated until the aiming point X_o, Y_o, Z_o is reached with a given accuracy.

Short Derivation of the Other Utilized Equations

If a plane wave is incident into a horizontally stratified ionosphere (without the earth magnetic field) one has:

$$n_o \sin\varphi_o = n_1 \sin\varphi_1 = \ldots = n_r \sin\varphi_r \qquad (32)$$

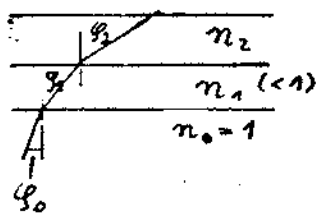

and

$$n_r = \sin\varphi_o \qquad (33)$$

because the ray is horizontal ($\varphi_r = 90^\circ$) at the height of reflection.

The refractive index n of a wave of frequency f is given by:

$$n(h) = \sqrt{1 - f_o^2(h)/f^2} \qquad (34)$$

The electron plasma frequency f_o is:

$$f_o^2 = \frac{N_e \cdot e^2}{4\pi^2 \cdot \varepsilon_o \cdot m_e} .$$

From (33) and (34) one obtains for the electron plasma frequency at the height of reflection:

$$f_{or} = f \cdot \cos \varphi_o \qquad (35)$$

If the ray path in the ionosphere is considered (see Fig.22) one has:

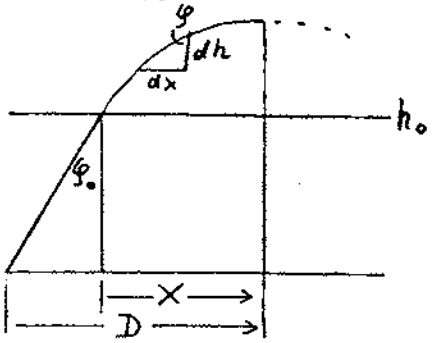

Fig.22

$$dx = tg\,\varphi(h)\,dh$$

and according to (32):

$$\sin\varphi(h) = \sin\varphi_o / n(h)$$

which leads to

$$dx = \frac{\sin\varphi_o}{\sqrt{n^2 - \sin^2\varphi_o}}\,dh \qquad (36)$$

Introducing n^2 according to (34) one has:

$$x = \sin\varphi_o \int_{f_o^2(h_o)} \frac{dh}{\sqrt{\cos^2\varphi_o - f_o^2(h)/f^2}} \qquad (37)$$

and the distance D associated with the vertex of the ray is:

$$D = h_o\,tg\,\varphi_o + x \qquad (38)$$

a) The Linear Layer

The linear layer is characterized by

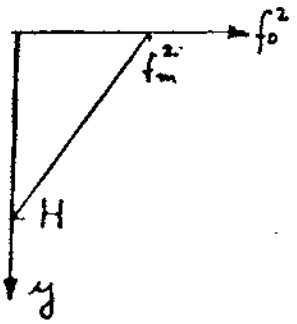

Fig.23

$$N_e \sim f_o^2 = f_m^2(1 - y/H) \qquad (39)$$

According to Fig.23 one finds the location of the vertex y_s from (35) and (39):

$$y_r = (1 - \cos^2\varphi_o/\eta^2)H, \quad \text{def. } \eta = f_m/f, \qquad (40)$$

and (37) can be written:

$$x = \sin\varphi_o \int_{H(1-\cos^2\varphi_o/\eta^2)}^{H} \frac{dy}{\sqrt{\cos^2\varphi_o - \eta^2(1 - y/H)}} = 2\frac{\sin\varphi_o \cdot \cos\varphi_o}{\eta^2} \cdot H \qquad (41)$$

The (horizontal) distance D to the vertex is

$$D = h_o \operatorname{tg} \varphi_o + 2H \cdot \frac{\sin \varphi_o \cdot \cos \varphi_o}{\eta^2} \qquad (42)$$

From (40) the height of reflection above the ground is:

$$h_r = h_o + H \cos^2 \varphi_o / \eta^2 \qquad (43)$$

If η^2 is eliminated from (42) and (43) one obtains:

$$\varphi_o = \operatorname{arctg}\left(\frac{D}{2h_r - h_o}\right) , \quad h_r > h_o \qquad (44)$$

(From 43 it follows $f \to 0$ for $h_r \to h_o$).

Consequently, if a ray is of such frequency that it reaches its vertex at the point D, h_r in an arbitrary linear layer the angle of incidence φ_o is given by (44) which is only a function of D, h_r and h_o.

Equ. (35) may be written:

$$f = f_{or}/\cos \varphi_o \qquad (35a)$$

If $\cos \varphi_o$ is determined from (44) and introduced in (35a) one has:

$$f = f_{or} \cdot \sqrt{1 + \frac{D^2}{(2h_r - h_o)^2}} \qquad (45)$$

which is the frequency leading to the reflection point D, h_r in a linear layer with the plasma frequency f_{or} at the height of reflection h_r and with the lower border h_o. If the above transmitting frequency is related to the plasma frequency at the height $h_o + H$ one obtains:

$$f = f_o\left\{h_o + H\right\} \sqrt{\frac{h_r - h_o}{H} \cdot \left[\frac{D^2}{(2h_r - h_o)^2} + 1\right]} \qquad (45a)$$

Two further relations shall only be mentioned: If one proceeds from the vertex of a ray in a linear layer horizontally by the finite distance Δx the corresponding Δy is (see Fig. 24):

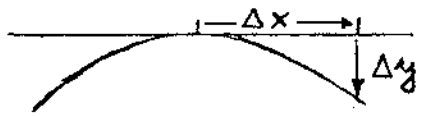

Fig.24

$$\Delta y = \frac{\eta^2}{4H^2 \sin^2 \varphi_o} \cdot (\Delta x)^2 \qquad (46)$$

The radius of the osculating circle at the vertex of the ray is given by:

$$|r| = \left|\frac{\sin \varphi_o}{dn/dh}\right|_{h=h_r} = 2H \cdot \frac{\sin^2 \varphi_o}{\eta^2} \quad . \qquad (47)$$

Finally one obtains from (35) the value of X at the height of reflection:

$$X_r = f_{or}^2 / f^2 = \cos^2 \varphi_o$$

which is according to (44):

$$X_r = 1/((D^2/(2h_r - h_o)^2) + 1). \qquad (48)$$

If X_r shall be greater than 0.9, which is a condition for sufficiently small Landau damping [8] one finds:

$$D \leq \frac{1}{3}(2h_r - h_o) \quad \text{for} \quad X_r \geq 0.9 \qquad (49)$$

in case of linear layers.

b) The Parabolic Layer

The parabolic layer is characterized by:

$$f_o^2 = f_c^2 (1 - (y/Y_m)^2) \qquad (50)$$

According to (37) and (38) one obtains:

$$D = h_o \operatorname{tg} \varphi_o + \frac{Y_m \sin \varphi_o}{\eta} \cdot \operatorname{Arth} (\cos \varphi_o / \eta) \qquad (51)$$

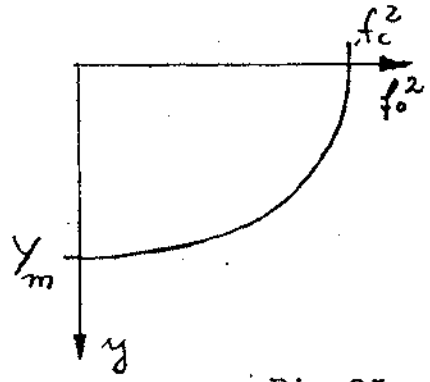

Fig.25

where $\eta = f_c/f$.

Equations (50), (33) and (34) yield with Fig.25 and with

$$h_r = h_o + Y_m - y_r$$

the height of reflection:

$$h_r = h_o + Y_m\left(1 - \sqrt{1 - \cos^2\varphi_o/\eta^2}\right) \qquad (52)$$

$\cos\varphi_o/\eta$ and $\sin\varphi_o$ may be evaluated from (52) and introduced in (51) to obtain a relation between D, h_o, Y_m, h_r and $f_r = 1/\eta = f/f_c$ as already mentioned on page 17, equ.(25) in connection with stability considerations of the reflection level.

Two further relations shall only be mentioned: If one proceeds from the vertex of a ray in a parabolic layer horizontally by the finite distance Δx the corresponding Δy is (see Fig. 24 on page 28):

$$\Delta y = Y_m\sqrt{1 - \cos^2\varphi_o/\eta^2}\cdot\left(\cosh\frac{\eta\cdot\Delta x}{Y_m\sin\varphi_o} - 1\right) \qquad (53)$$

The osculating circle at the vertex of the ray is given by:

$$|r| = \left|\sin\varphi_o/(dn/dh)\right| = \frac{Y_m\sin^2\varphi_o}{\sqrt{\eta^2 - \cos^2\varphi_o}} \qquad (54)$$

c) The Exponential Layer

An exponential layer may be defined by:

$$\begin{aligned} f_o^2(h) &= f_o^2(h_o)\, e^{\alpha\cdot(h - h_o)}, & h \geq h_o \\ f_o^2 &= 0 & \text{for} \quad h < h_o \end{aligned} \qquad (55)$$

If the plasma frequencies are known in two different heights e.g. at h_o and at h_m one obtains for α :

$$\alpha = \frac{\ln\left[\left(f_o^2(h_m)\ /\ f_o^2(h_o)\right]\right.}{h_m - h_o} \qquad (56)$$

Abbreviating:

$$\xi = f_o(h_o)/f$$

one obtains:

$$D = tg\varphi_o\left(h_o + \frac{2}{\alpha}\,\mathrm{Arth}\sqrt{1 - \xi^2/\cos^2\varphi_o}\right) \qquad (57)$$

and the height of reflection is:

$$h_r = h_o + \frac{1}{\alpha}\ln(\cos^2\varphi_o/\xi^2) \qquad (58)$$

If one proceeds from the vertex of a ray in an exponential layer horizontally by the finite distance Δx (see Fig. 24 on page 28) the corresponding Δy is:

$$y = \frac{2}{\alpha}\ln\left[\cosh\left(\frac{\alpha\cdot\Delta x}{2\cdot tg\,\varphi_o}\right)\right] \qquad (59)$$

The radius of the osculating circle at the vertex of the ray is:

$$|r| = \left|\sin\varphi_o/(dn/dh)\right|_{h=h_r} = \frac{2}{\alpha}\,tg^2\varphi_o \qquad (60)$$

<u>The Equivalent Linear Layer</u>

An arbitrary electron profile may be given and a transmitting frequency may exist for which the ray has its vertex at the height h_r. With the aid of the equivalent linear layer the frequency f_h belonging to that ray may be estimated.

The equivalent linear layer has the same electron density at h_r and its electron content up to h_r is the same as that of the given layer.

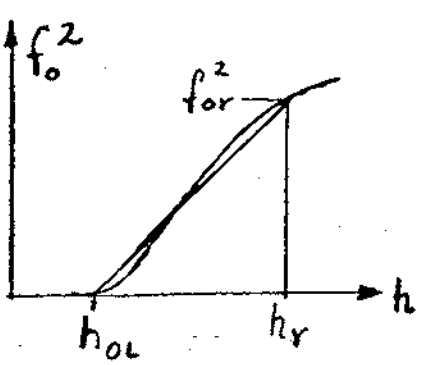

A linear layer may be described by:

$$f_o^2 = a\,h - b \qquad (61)$$

where a and b are constants. In case of an equivalent linear layer a and b have to be determined such that

the area of the given profile:

$$F = \int_0^{h_r} f_o^2(h) \cdot dh \qquad (62)$$

is the same as that of the linear profile

$$F = \int_{h_{oL}=b/a}^{h_r} (ah - b)\, dh. \qquad (63)$$

From (63) it follows

$$a^2 h_r^2 - 2abh_r + b^2 - 2aF = 0 \qquad (64)$$

and from the equality of the plasma frequencies at the height of reflection it follows:

$$ah_r = f_{or}^2 + b \qquad (65)$$

and from (64) and (65):

$$a = f_{or}^4/2F \qquad (66)$$

b follows from (66) and (61):

$$b = f_{or}^4 h_r/2F - f_{or}^2. \qquad (67)$$

Finally the lower boundery h_{oL} of the equivalent linear layer is given by

$$h_{oL} = b/a = h_r - 2F/f_{or}^2 \qquad (68)$$

which was already introduced on page 21, equ. (29).

The Equivalent Linear Layer if it Replaces a Parabolic Layer

If the parabolic layer is normalized to $f_c^2 = 1$ one has:

$$f_o^2(y) = 1 - (y/Y_m)^2 \qquad (69)$$

and the area from the point of reflection at y_r to $y = Y_m$ is given by:

$$F = \int_{y_r}^{Y_m} (1 - (y/Y_m)^2) \cdot dy = \frac{2}{3}Y_m - y_r + \frac{y_r^3}{3Y_m^2} \qquad (70)$$

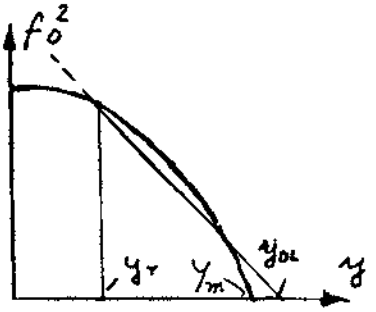

If (70) is introduced into (68) and if (69) is used one obtains for the lower border of the equivalent linear layer:

$$h_{oL} = h_r - \frac{2}{1-(y_r/Y_m)^2} \left(\frac{2}{3} Y_m - y_r + \frac{y_r^3}{3Y_m^2} \right) \qquad (71)$$

where y_r may still be replaced by the height of reflection h_r and the height of the lower border of the parabolic layer h_{op}:

$$y_r = h_{op} + Y_m - h_r \,. \qquad (72)$$

If $h_o = h_{oL}$ is used in equ. (44) to determine the equivalent linear layer approximation of φ_o one immediately obtains an estimate of the frequency which has its vertex at the height h_r in the given parabolic layer:

$$f_h \approx \frac{f_c \sqrt{1 - (y_r/Y_m)^2}}{\cos \varphi_o} = f_c \sqrt{1 - \left(\frac{y_r}{Y_m}\right)^2} \cdot \sqrt{1 + \frac{D^2}{(2h_r - h_o)^2}} \qquad (73)$$

The heights which are really obtained when $\eta = f_c/f_h$ of (73) and φ_o of (44) are introduced in (52) have been compared in the first part of this paper with the height h_r (at distance D) which was aimed at.

<u>The Equivalent Linear Layer if it Replaces an Exponential Layer</u>

In case of an exponential layer (with a lower boundery) as given by equ.(55) the height h_{oL} is found to be:

$$h_{oL} = h_r + \frac{2}{\alpha} \left(\frac{f_o^2(h_o)}{f_{or}^2} - 1 \right) \qquad (74)$$

which may be replaced by:

$$h_{oL} = h_r - \frac{2}{\alpha} \qquad \text{for} \qquad \frac{f_o^2(h_o)}{f_{or}^2} \ll 1 \qquad (74a)$$

If $h_o = h_{oL}$ is introduced into (44) one obtains:

$$f_h = \frac{f_o(h_o) \cdot e^{\frac{\alpha}{2}(h_r - h_o)}}{\cos \varphi_o} \qquad (75)$$

$$= f_o(h_o) \cdot e^{\frac{\alpha}{2}(h_r - h_o)} \sqrt{1 + \frac{D^2}{(2h_r - h_o)^2}}$$

References

[1] Stubbe, P., H. Kopka and G. Rose: Rocket experiments in conjunction with the ionospheric modification experiment in northern Norway. Proc. European Sounding-Rocket, Balloon and Related Research, with Emphasis on Experiments at High Latitudes, Eds. T. Halvorsen and B. Battrich, ESA SP-135, 107-111 (1978).

[2] Stubbe, P. and H. Kopka: Ionospheric modification experiments in northern Scandinavia - a description of the heating project -. Internal Report MPAE-W-02-79-04, 1 - 13 (1979).

[3] Fejer, J.A. and Egil Leer: Excitation of parametric instabilities by radio waves in the ionosphere. Radio Science 7, Nr. 4, 481-491 (1972).

[4] Jones, R.M. and Judith J. Stephenson: A versatile three-dimensional ray tracing computer program for radio waves in the ionosphere. OT Techn. Report 75-76, Institute for Telecommunication Sciences, Boulder, Colorado, (Oct. 1975).

[5] Bruce L. Cragin: Report on ray-tracing program for project heating. Private Communication.

[6] Ma, M.T.: Theory and application of antenna arrays. A Wiley-Interscience Publication, John Wiley and Sons, New York - London - Sidney - Toronto (1974).

[7] Meinke/Gundlach: Taschenbuch der Hochfrequenztechnik, Springer Verlag, P. 537 (1968).

[8] Grandal, B.: Ray tracing of the heating wave and related problems in using sounding rocket probes in the German artificial ionosphric modification experiment planned at Ramfjordmoen. Internal Report E-273, Reference: Job 335/172, Forsvarets Forskningsinstitut, NDRE, Postbox 25-2007 Kjeller Norge (1977).

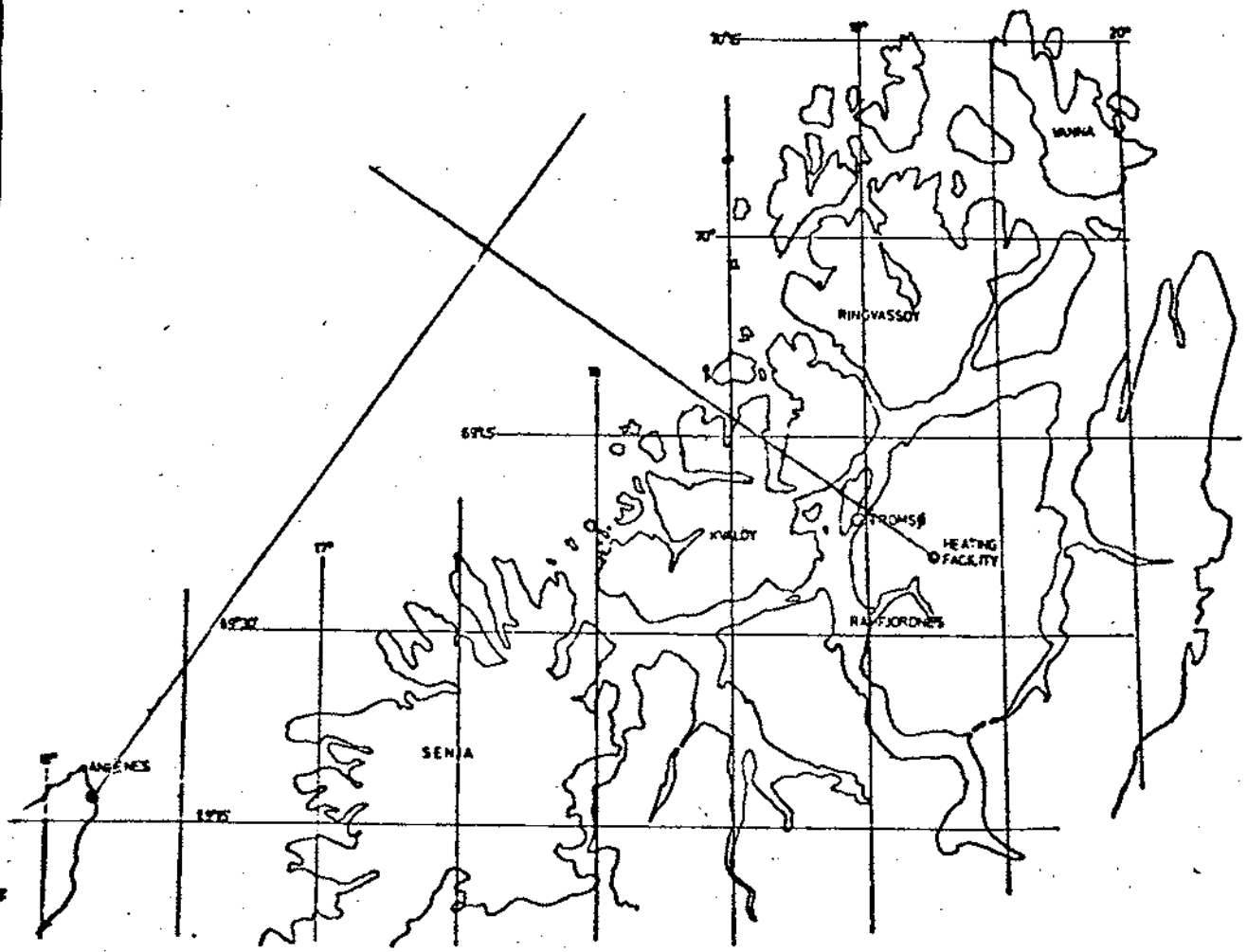

Fig. 1: Illustration of the rocket trajectory and the heating beam

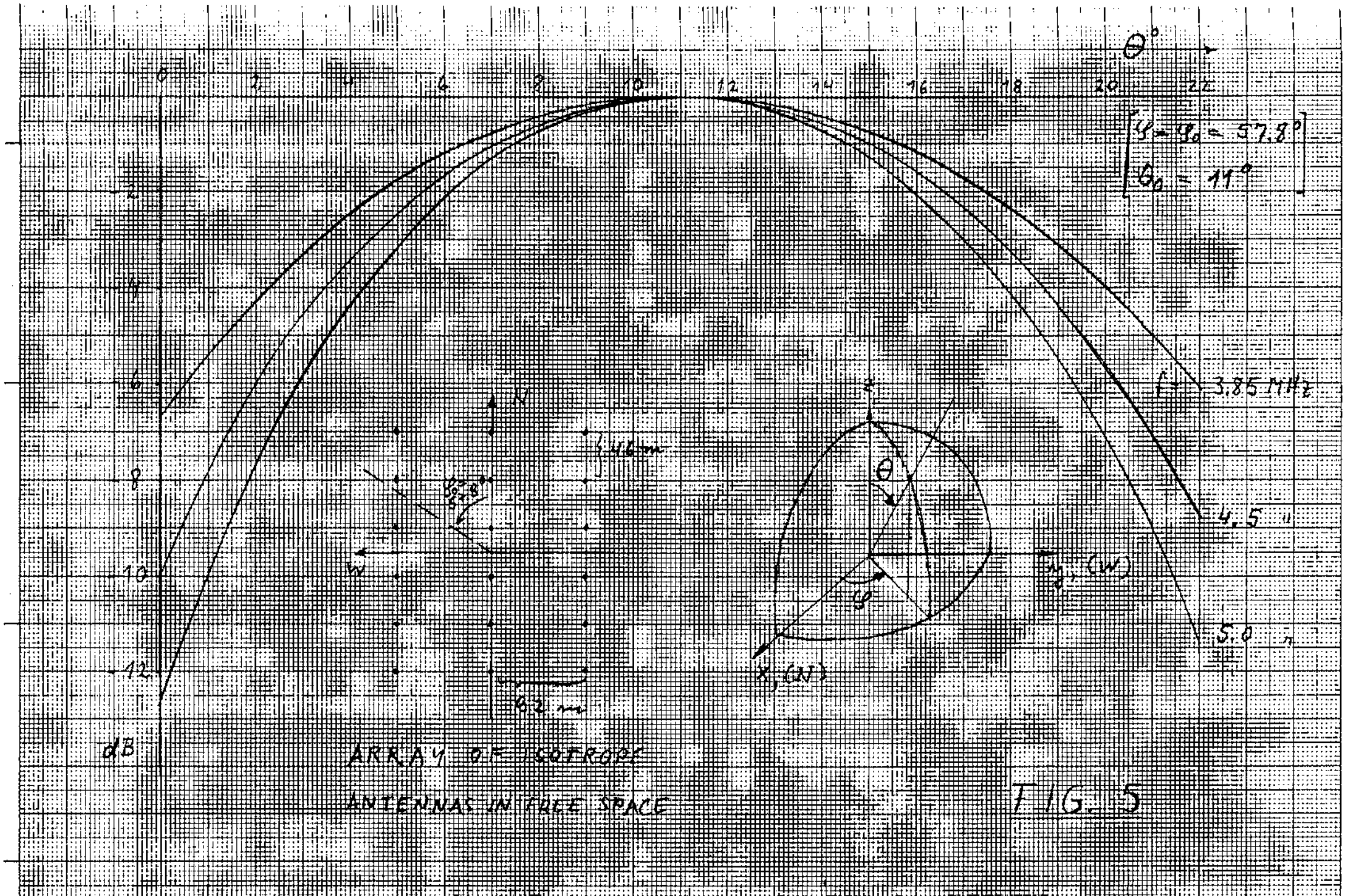

ARRAY OF COFROPE

ANTENNAS IN FREE SPACE

FIG. 5

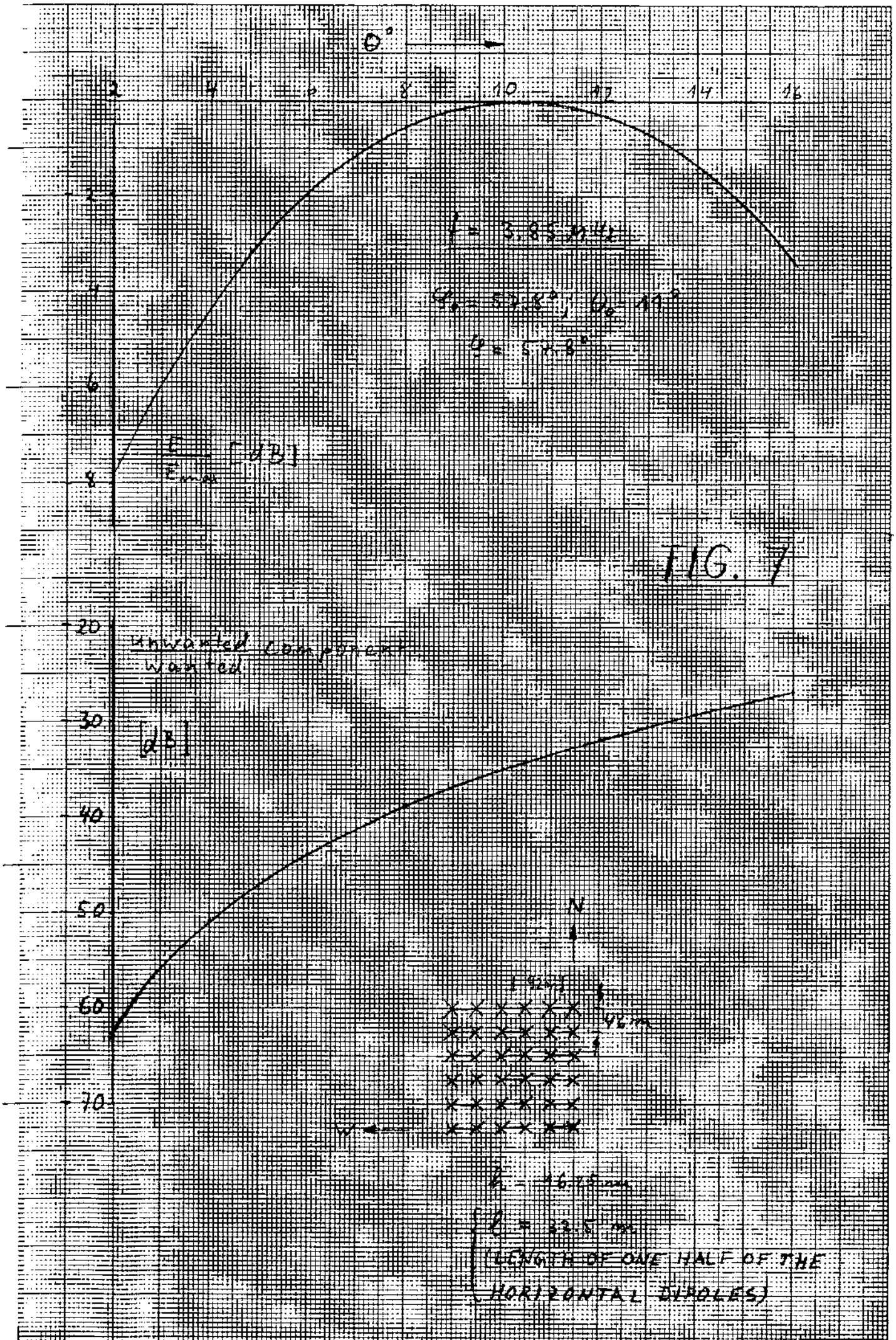

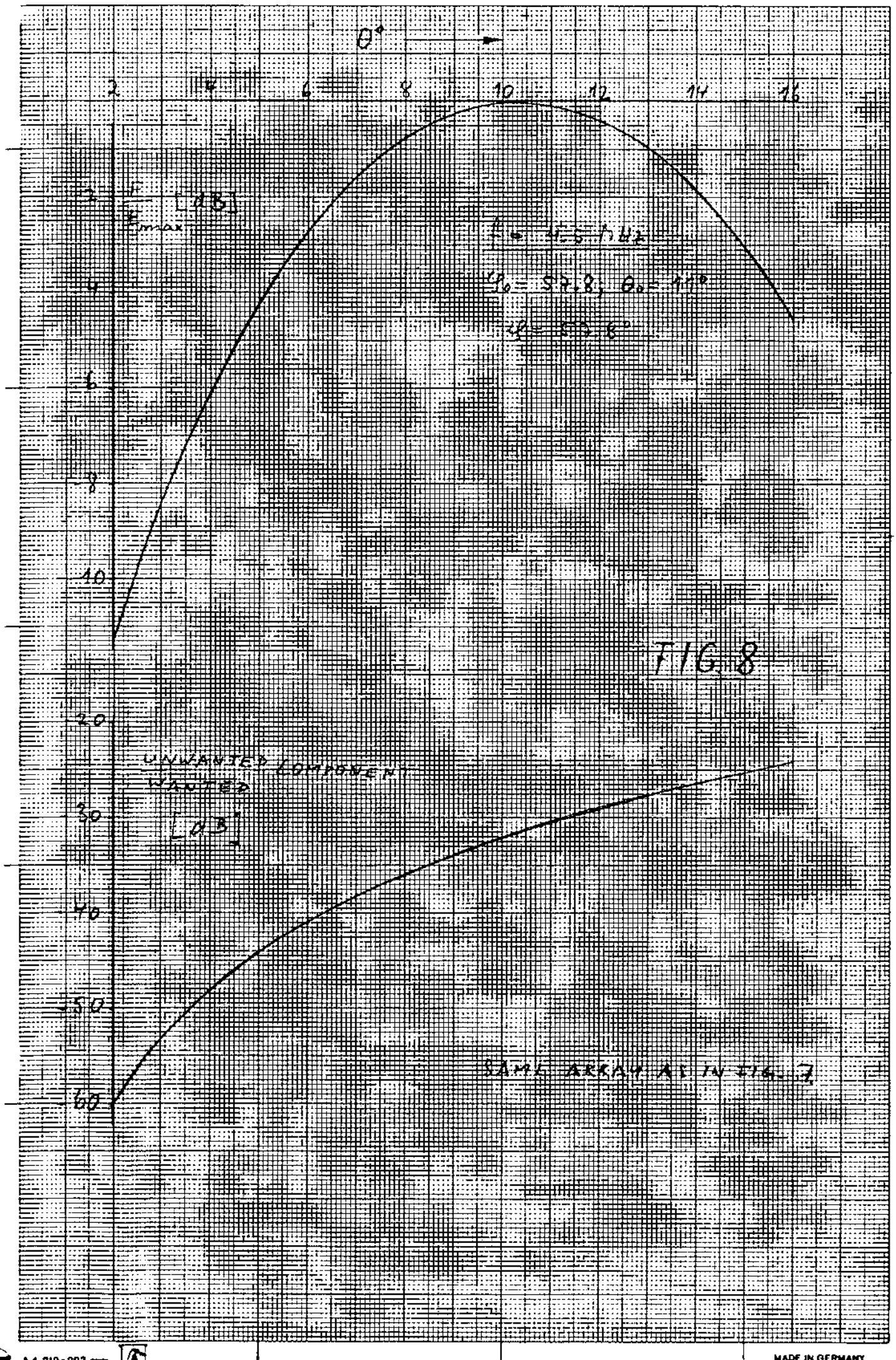
θ°
2
4
6
8
10
12
14
16
-2
-4
-6
-8
-10
-20
-30
-40
-50
-60
$\frac{E}{E_{max}}$ [dB]
f = 3.5 MHz
φ_0 = 322°, θ_0 = 11°
φ_0 = 50.6°
UNWANTED COMPONENT / WANTED [dB]
SAME ARRAY AS IN FIG. 7

FIG. 8

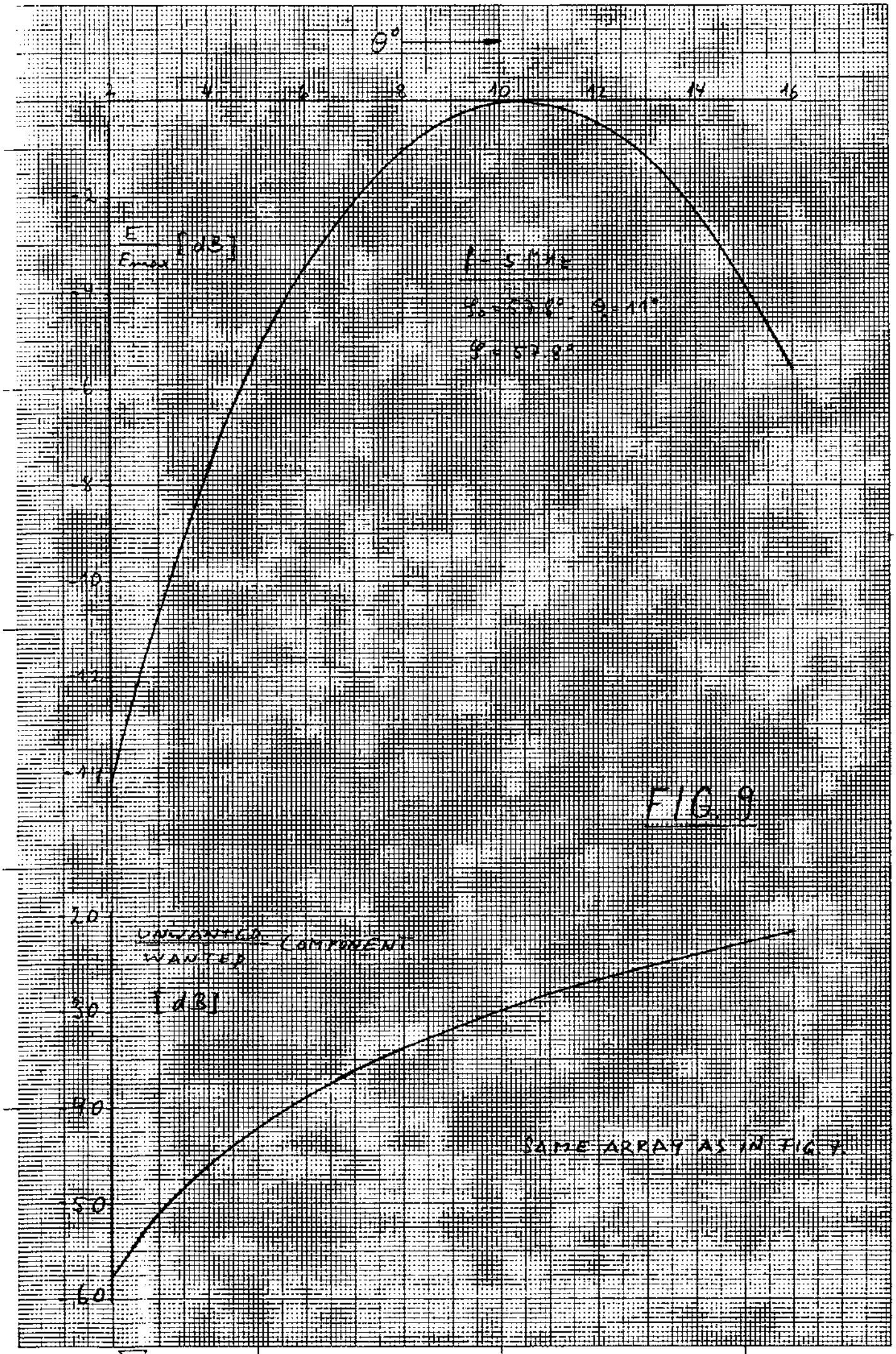

FIG. 9

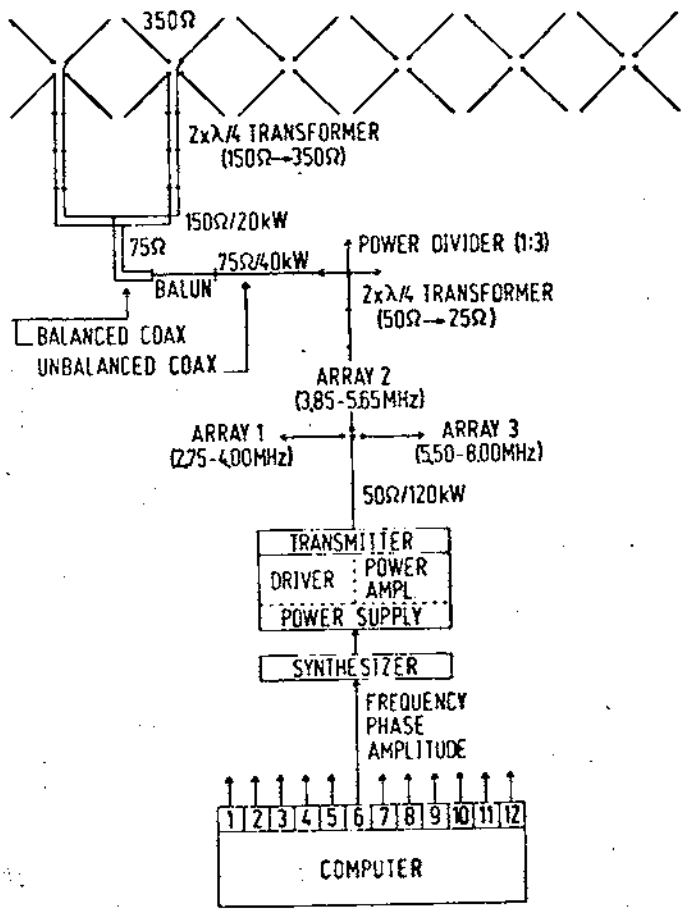

Fig. 10: Functional diagram of the heating equipment

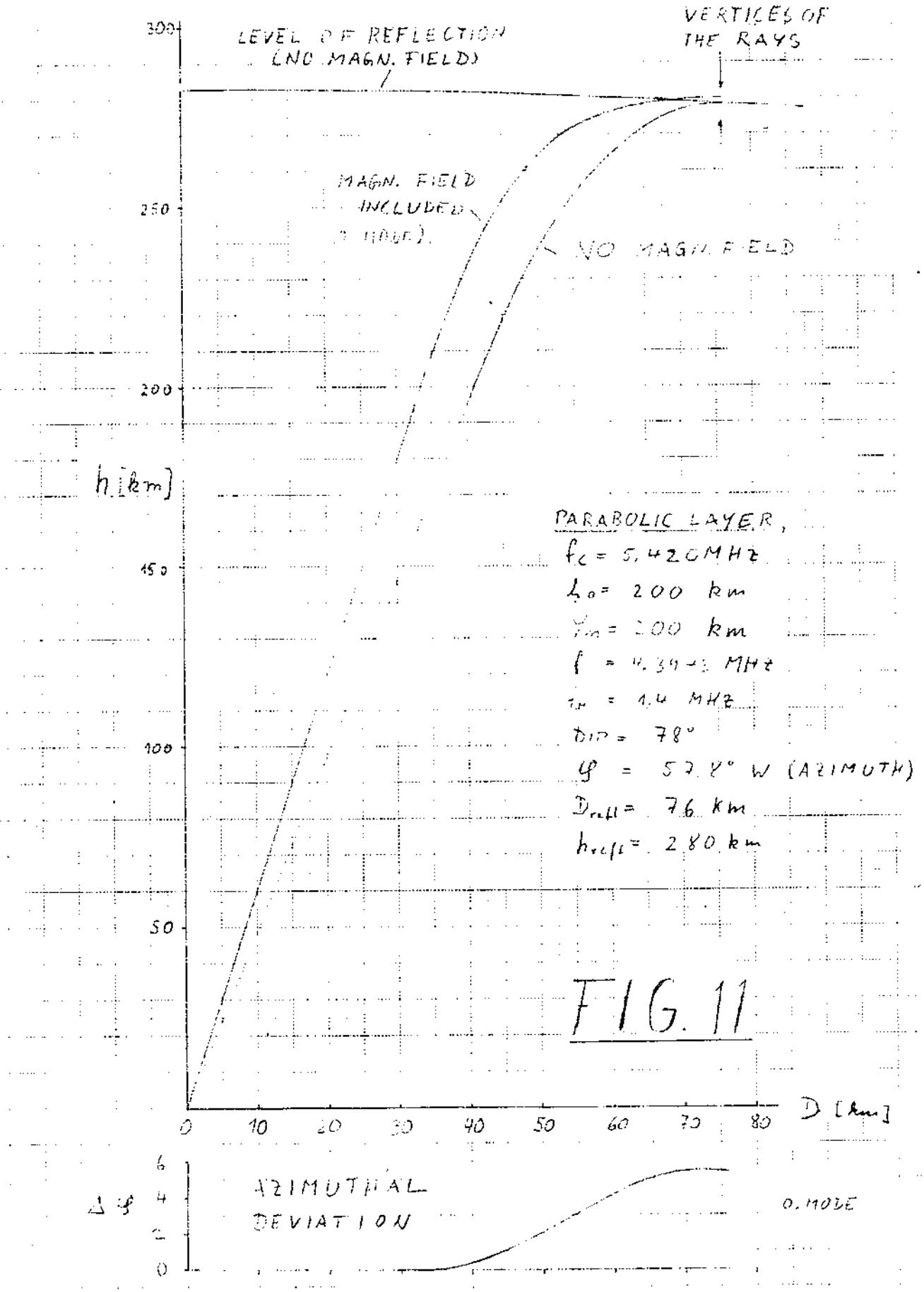
LEVEL OF REFLECTION (NO MAGN. FIELD)
VERTICES OF THE RAYS
MAGN. FIELD INCLUDED
NO MAGN. FIELD
h [km]
300
250
200
150
100
50
0
10
20
30
40
50
60
70
80
D [km]
PARABOLIC LAYER,
f_c = 5.420 MHz
h_0 = 200 km
y_m = 200 km
f = 4.39 MHz
f_H = 1.4 MHz
DIP = 78°
φ = 57.8° W (AZIMUTH)
D_{refl} = 76 km
h_{refl} = 280 km
$\Delta\varphi$
6
4
2
0
AZIMUTHAL DEVIATION
O. MODE

FIG. 11

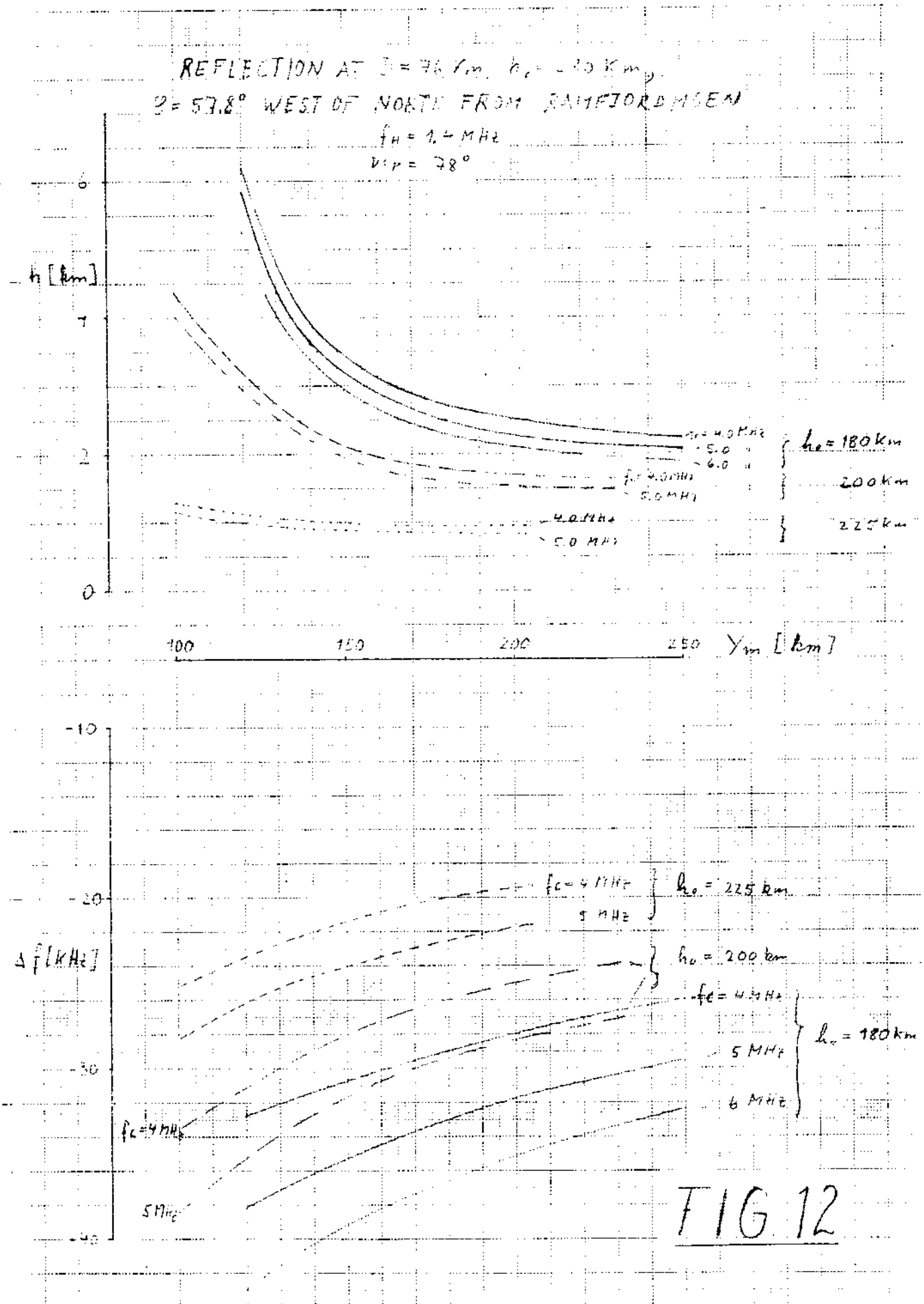
REFLECTION AT D = 76 Km, h = 70 Km
Ψ = 57.8° WEST OF NORTH FROM TRONDHEIM
fH = 1.4 MHz
Dip = 78°
h [km]
6
4
2
0
fc = 4.0 MHz
5.0 "
6.0 "
fc = 4.0 MHz
5.0 MHz
4.0 MHz
5.0 MHz
he = 180 km
200 km
225 km
100
150
200
250
Ym [km]
-10
-20
-30
Δf [kHz]
fc = 4 MHz
5 MHz
h0 = 225 km
h0 = 200 km
fc = 4 MHz
5 MHz
6 MHz
h0 = 180 km
fc = 4 MHz
5 MHz

FIG 12

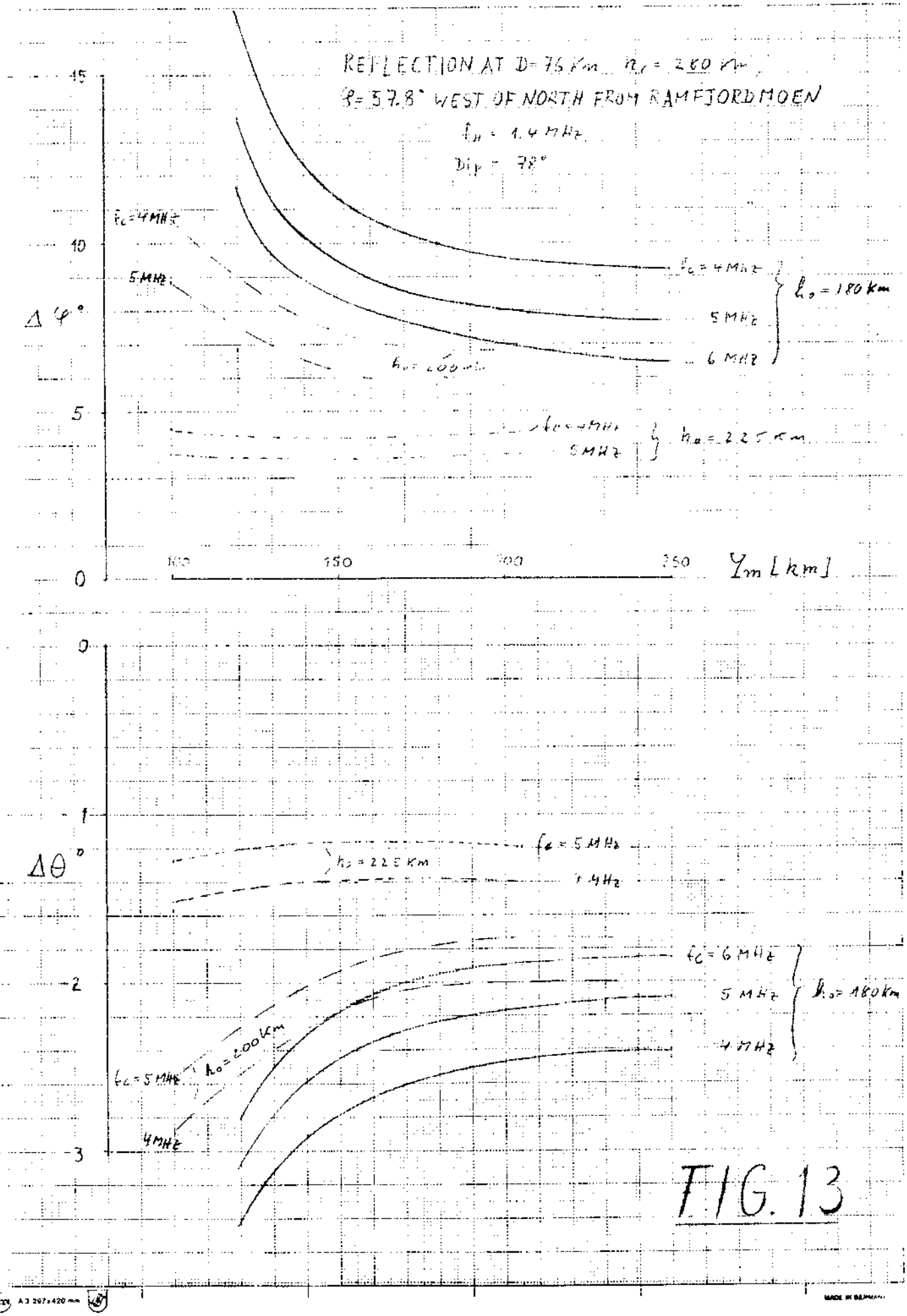
REFLECTION AT D= 75 Km h_r = 260 Km
R= 57.8° WEST OF NORTH FROM KAMFJORDMOEN
f_H = 1.4 MHz
Dip = 78°
$\Delta\varphi$°
15
10
5
0
f_c=4MHz
5MHz
h_o=200 Km
f_c=4MHz
5MHz
6 MHz
h_o=180 Km
h_o=225 Km
100
150
200
250
Y_m [km]
$\Delta\theta$°
0
1
2
3
h_2=225 Km
f_c=5MHz
4MHz
f_c=6MHz
5 MHz
4 MHz
h_o=180 Km
f_c=5MHz
h_o=200 Km
4MHz

FIG. 13

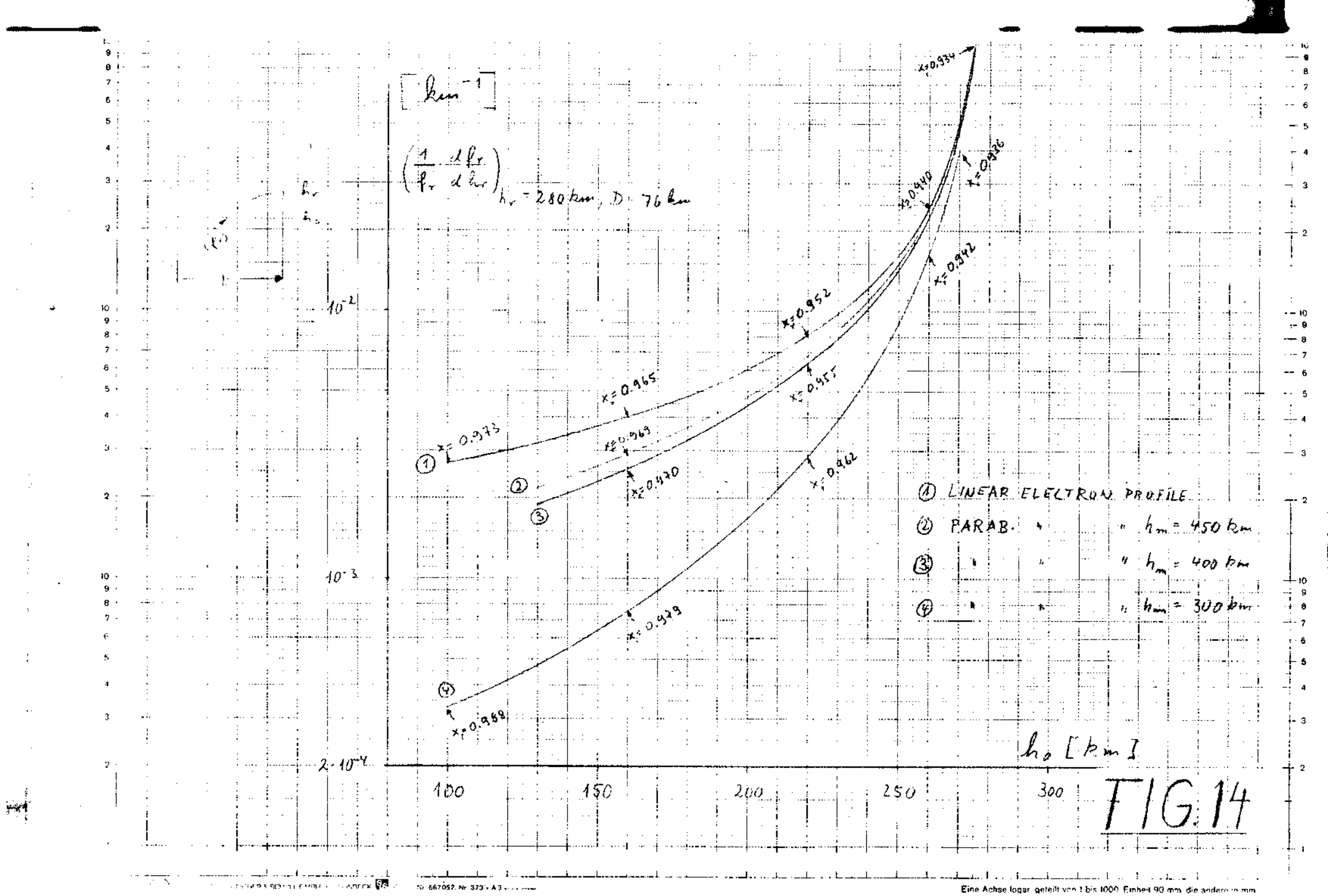

FIG. 14

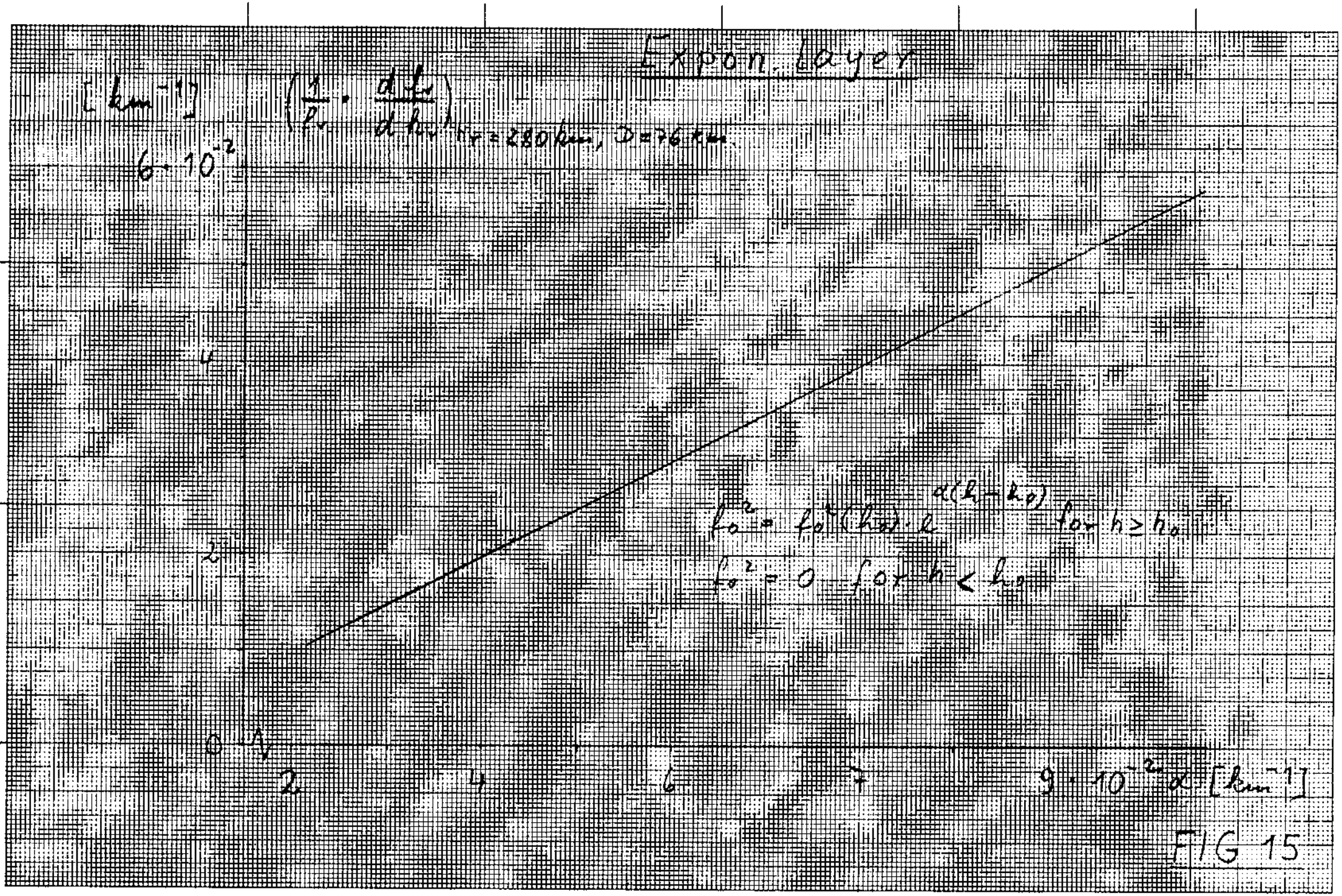
Exponential layer
$\left(\frac{1}{f_v}\cdot\frac{df_v}{dh_v}\right)_{h_v=280\,km,\ D=76\,km}$ [km⁻¹]
6·10⁻²
4
2
0
2
4
6
7
9·10⁻²
α [km⁻¹]
$f_o^2 = f_o^2(h_o)\cdot e^{\alpha(h-h_o)}$ for $h \geq h_o$
$f_o^2 = 0$ for $h < h_o$

FIG 15

PARABOLIC LAYER

(CORRECTION TERMS)

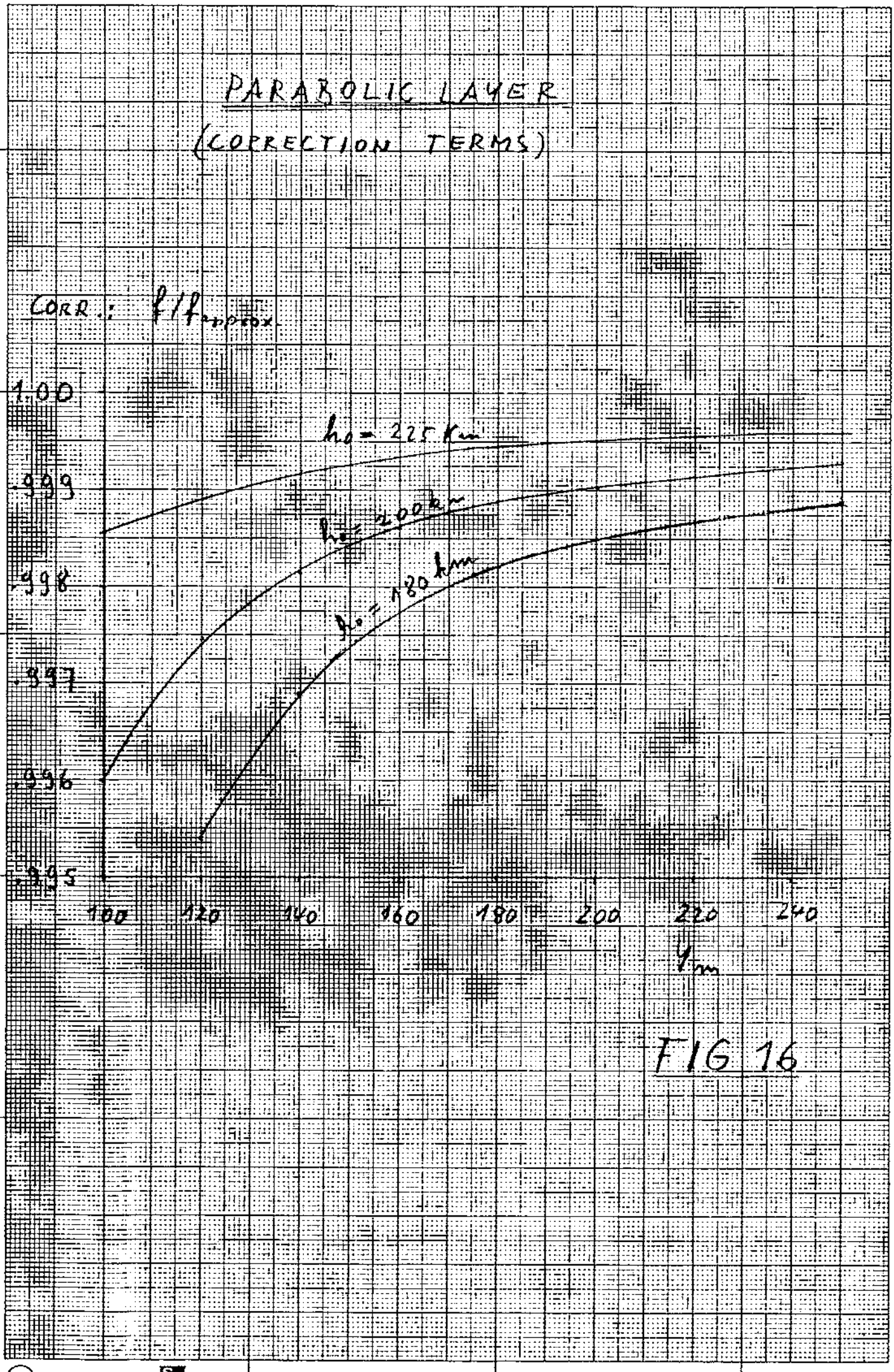

FIG 16

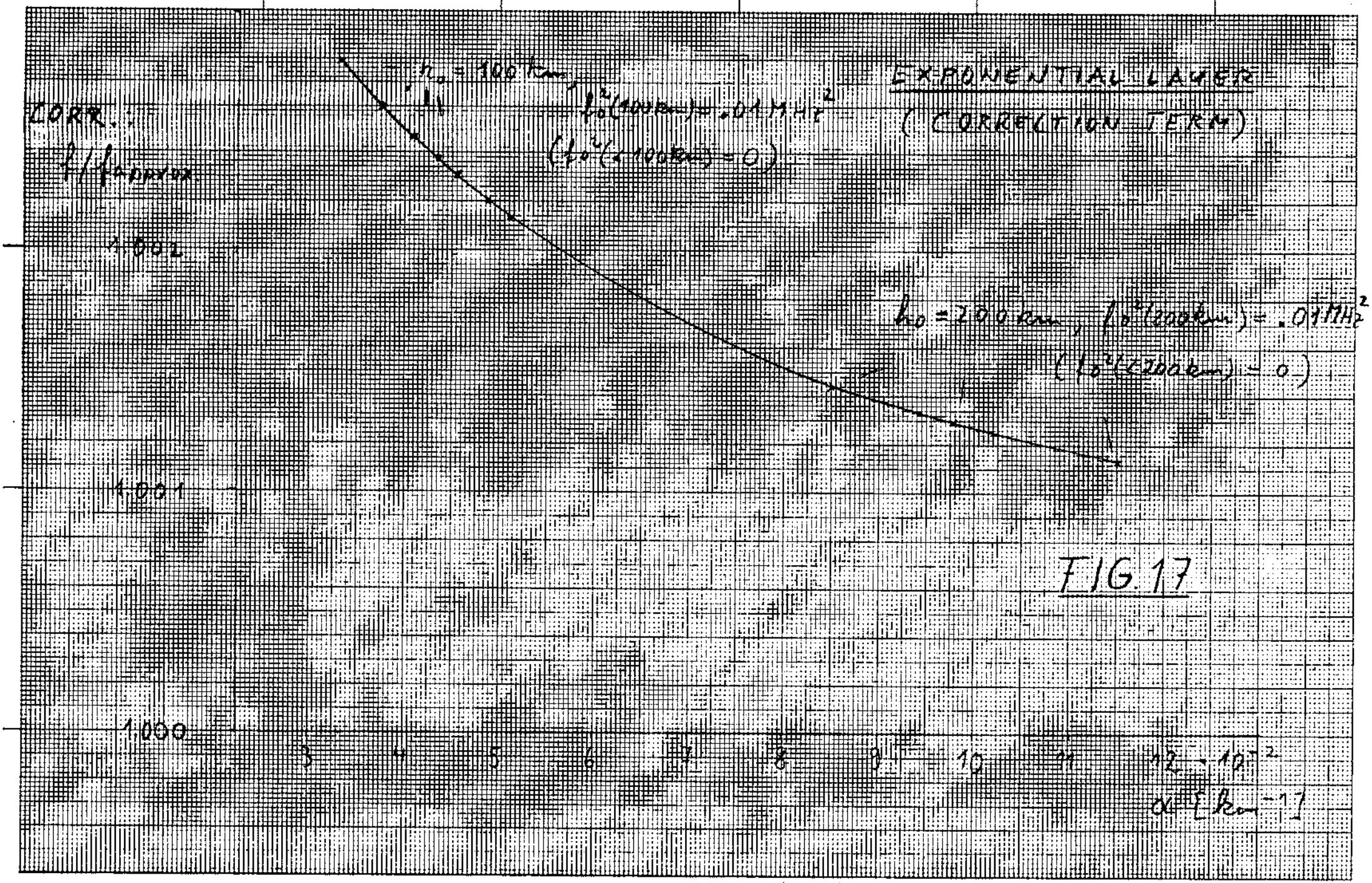
EXPONENTIAL LAYER
(CORRECTION TERM)
CORR.:
$f/f_{h=\infty}$
1.002
1.001
1.000
$h_0 = 100$ km, $f_0^2(100\,km) = .01\,MHz^2$
$(f_0^2(<100\,km) = 0)$
$h_0 = 200$ km, $f_0^2(200\,km) = .01\,MHz^2$
$(f_0^2(<200\,km) = 0)$
3 4 5 6 7 8 9 10 11 $n^2 \to 10^{-2}$
$\alpha = [km^{-1}]$

FIG. 17

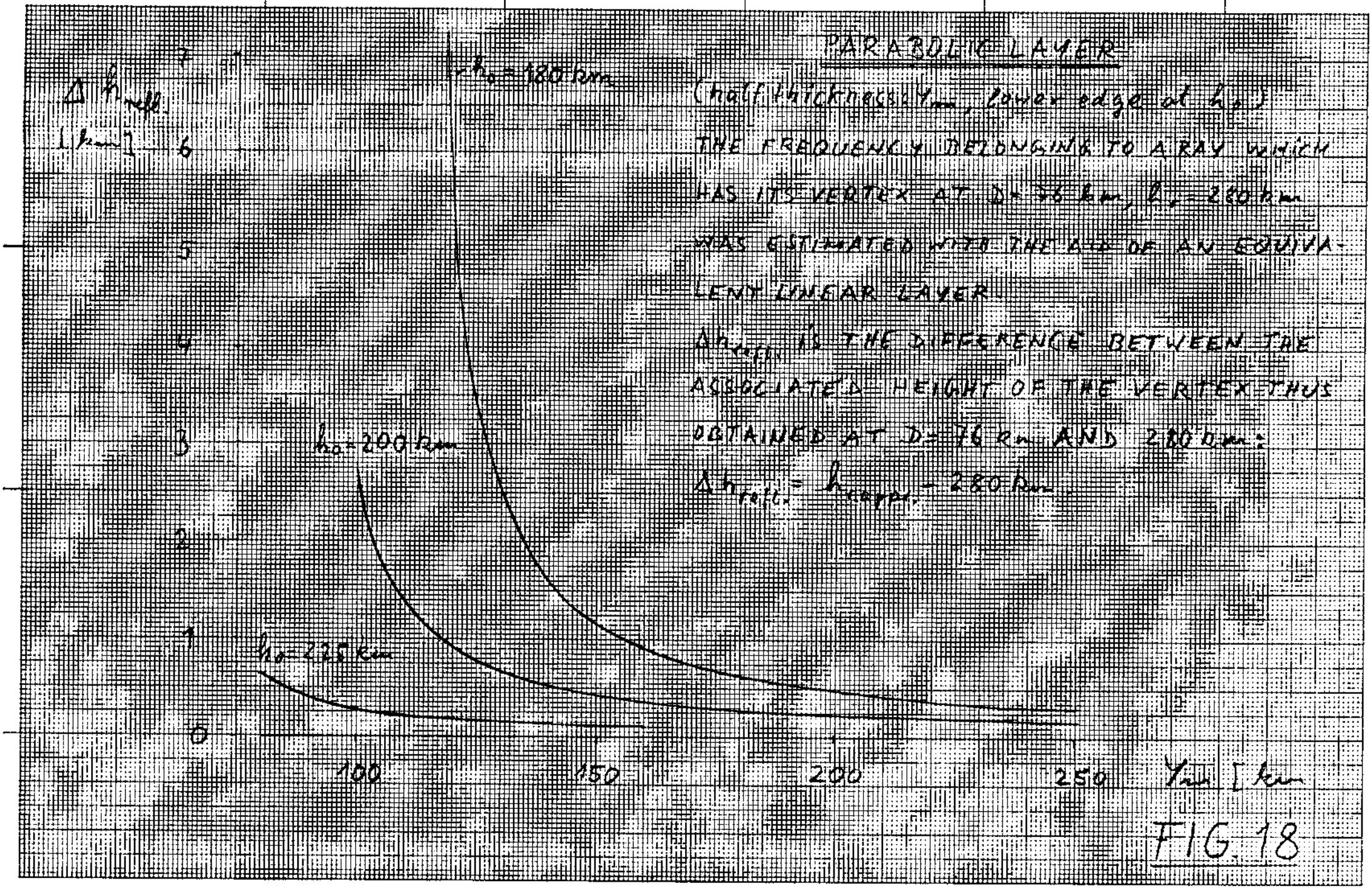
PARABOLIC LAYER
(half thickness: Ym, lower edge at h_o)
THE FREQUENCY BELONGING TO A RAY WHICH HAS ITS VERTEX AT D = 36 km, h_v = 260 km WAS ESTIMATED WITH THE AID OF AN EQUIVALENT LINEAR LAYER
$\Delta h_{reflr.}$ IS THE DIFFERENCE BETWEEN THE ASSOCIATED HEIGHT OF THE VERTEX THUS OBTAINED AT D = 36 km AND 260 km:
$\Delta h_{reflr.} = h_{vertex} - 260$ km
$\Delta h_{reflr.}$ [km]
h_o = 120 km
h_o = 200 km
h_o = 225 km
7
6
5
4
3
2
1
0
100
150
200
250
Ym [km]

FIG. 18

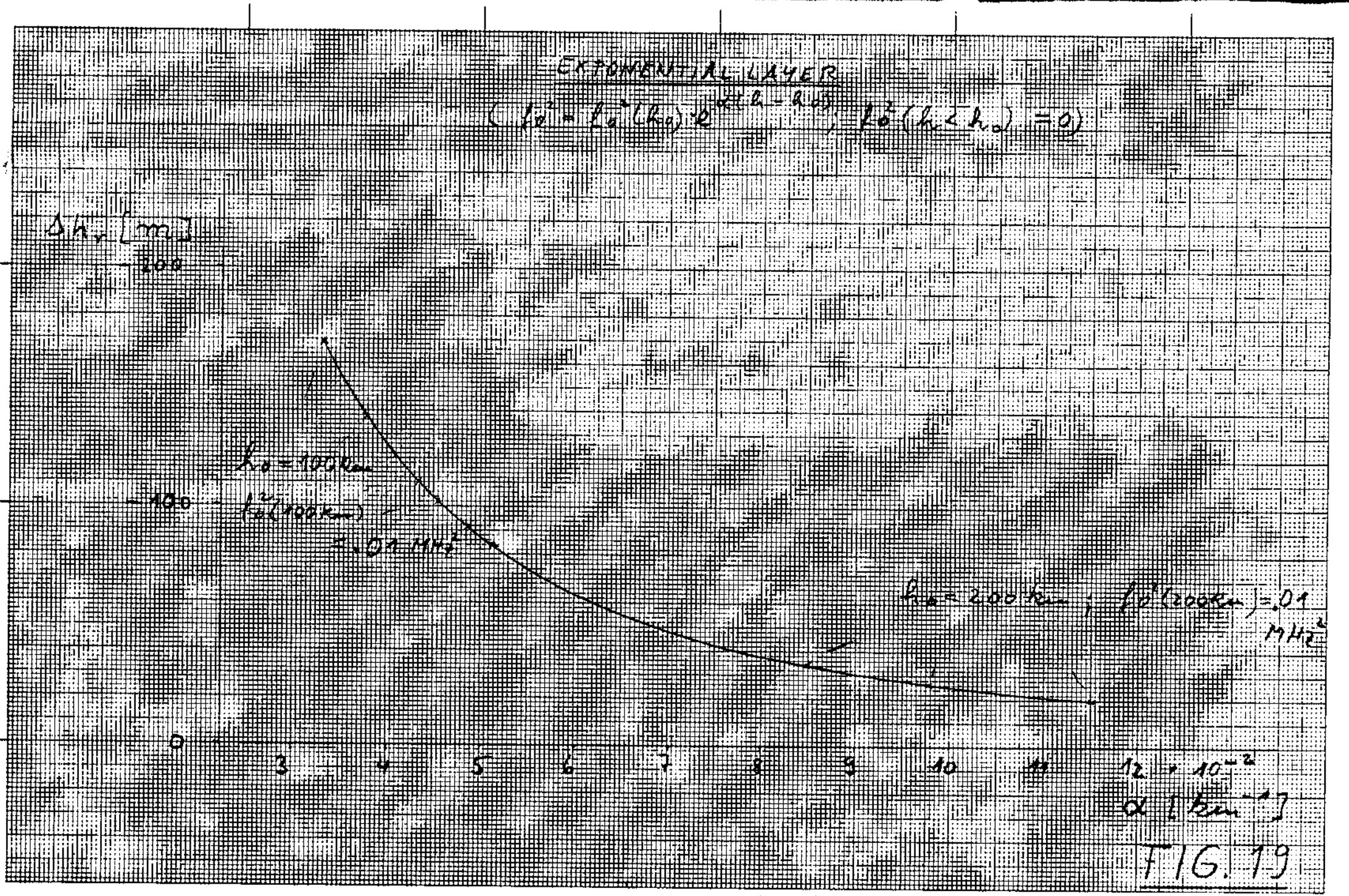
EXPONENTIAL LAYER
$(f_0^2 = f_{0_0}^2 (h_0) \cdot 2^{\alpha (h - h_0)}, \; f_0^2 (h < h_0) = 0)$
Δh_v [m]
200
100
0
$h_{0_0} = 100$ km
f_0^2 (100 km) = .01 MHz^2
$h_{0_0} = 200$ km ; f_0^2 (200 km) = .01 MHz^2
3
4
5
6
7
8
9
10
11
12
$\cdot 10^{-2}$
α [km^{-1}]

FIG. 19

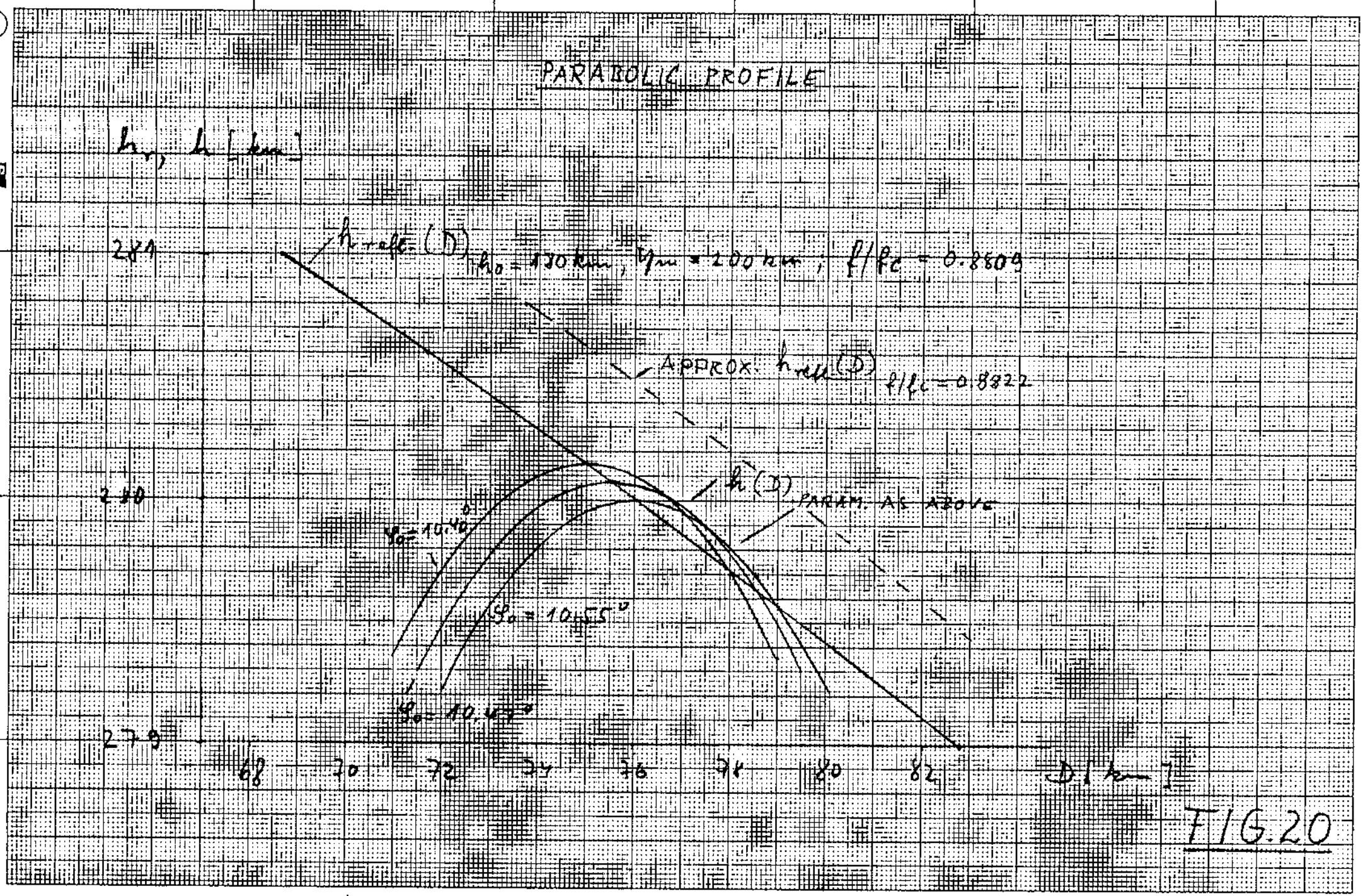
PARABOLIC PROFILE
h, L [km]
281
280
279
68
70
72
74
76
78
80
82
D [km]
h_ref (D) h₀ = 130 km, h_m = 200 km; f/f_c = 0.8809
APPROX. h_ref (D) f/f_c = 0.8822
h (D) PARAM. AS ABOVE
ϑ₀ = 10.40°
ϑ₀ = 10.45°
ϑ₀ = 10.47°

FIG. 20

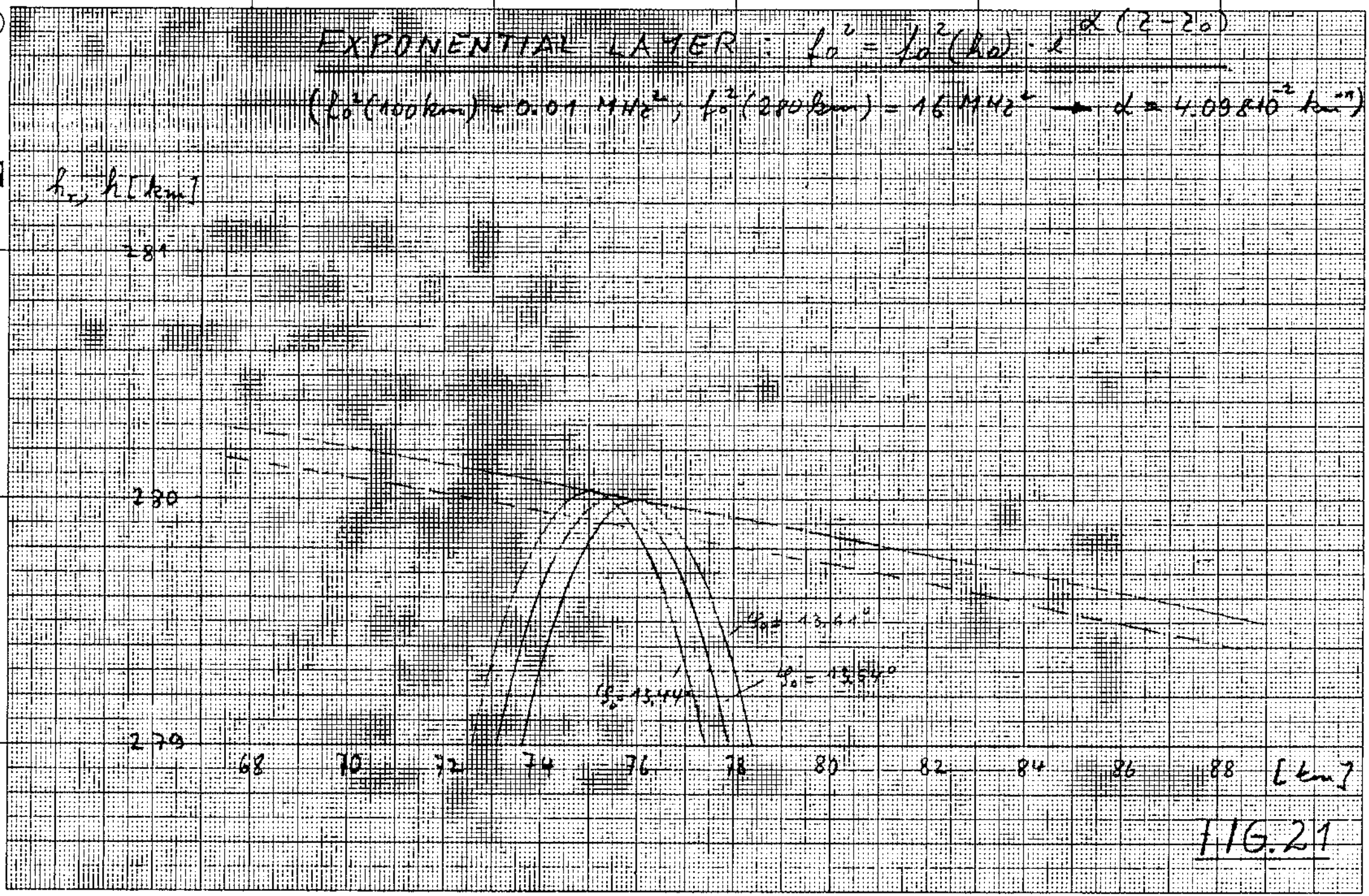
EXPONENTIAL LAYER : $f_o^2 = f_{o0}^2 (h_{o0}) \cdot e^{\alpha (z - z_0)}$
($f_o^2(100\,km) = 0.01\ MHz^2$; $f_o^2(280\,km) = 16\ MHz^2$ → $\alpha = 4.098 \cdot 10^{-2}\ km^{-1}$)
h_r, h [km]
281
280
279
68
70
72
74
76
78
80
82
84
86
88
[km]
$\varphi_0 = 13,44°$
$\varphi_0 = 13,54°$
$\varphi_0 = 13,44°$

FIG. 21